Inorganic Chemistry

ARTICLE

pubs.acs.org/IC

Synthesis and Properties of Metal−Ligand Complexes with Endohedral Amine Functionality

Amber M. Johnson, Orly Moshe, Ana S. Gamboa, Brian W. Langloss, John F. K. Limtiaco, Cynthia K. Larive, and Richard J. Hooley*

Department of Chemistry, University of California, Riverside, California 92521, United States

Supporting Information

ABSTRACT: A series of tetracationic M_2L_4 palladium-pyridyl complexes with endohedral amine functionality have been synthesized. The complexes were analyzed by NMR techniques (including Diffusion NMR and 2D NOESY), electrospray ionization (ESI) mass spectrometry, and X-ray crystallography. The solid state analysis shows a large change in crystal morphology upon introduction of the endohedral amine groups, caused by deleterious interactions between the amines and the triflate counterions from the coordination process. Combination of different ligands allows analysis of ligand exchange rates via NMR analysis, with half-lives on the order of 3 h, independent of the donor properties of the ligand. Self-sorting behavior is observed, with more electron-rich ligands being favored. The amine-containing and extended complexes are strongly fluorescent, giving quantum yields of up to 83%.

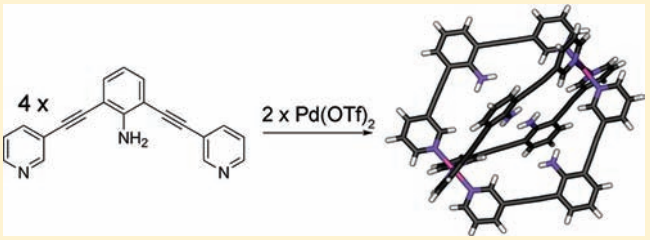

INTRODUCTION

The construction of self-assembled complexes with interior cavities of defined size and shape is a rapidly advancing field of research. Flat organic ligands can be coordinated by metal ions,[1,2] forming polyhedra of various geometries[3] with the metals at the vertices[4] and the ligands forming the faces.[5] A variety of metal−ligand contacts are known, from octahedral iron and gallium complexes with β-diketones[6] and catecholates,[7] to pyridylimine complexes coordinated by iron and nickel,[8] among others. In addition, complexes of pyridine or acetylene ligands with square planar palladium[9,10] and platinum[11] species give rise to a significant number of self-assembled polyhedra. These polyhedra contain interior cavities that are capable of noncovalently binding suitably sized guests and so can act as excellent mimics of the behavior of enzymes. As well as host:guest chemistry,[6−9,12] biomimetic reactions[13] and catalysis[14] are possible. Where the analogy with enzymes falters is in the presence (or lack thereof) of appended *functionality*. Few assemblies are known that display groups of any kind on the interior of the complex.[15] Most notably, Fujita has displayed alkylammonium cations, fluorocarbons, and aromatic groups on the interior of a self-assembled $M_{12}L_{24}$ nanocomplex. Metal−ligand complexes that introvert catalytically active groups such as amines or carboxylic acids are unknown, although there are examples of organic hosts that can mimic the behavior of amino acid side chains in enzyme mechanisms in this way.[16] In fact, ligand derivatization in any form is still underutilized, although examples of externally functionalized complexes have been recently reported.[17]

The reasons for this are many; the efficient self-assembly of metallocomplexes comes from the rigidity of the ligands that is often conferred by flat aromatic or acetylenic groups. Correspondingly, pointing a functional group perpendicular to the ligand is most difficult. Even if this is achieved, the self-assembly process requires donor ligands to coordinate to the metal vertices, and so discriminating between "structural" lone pairs (to construct the host) and "active" lone pairs (to display to the interior cavity) is of vital importance. This can be achieved by postsynthetic modification of metal−organic frameworks in the solid state,[18] but the reversibility of self-assembled solution-phase complexes renders this strategy impractical. The attachment of functional groups to self-assembled structures is extremely desirable, as it would enable the variation of ligand electronics and provide methods for analysis of the self-assembly and ligand exchange process, not to mention promoting reactivity, catalysis, and sensing. In this report, we discuss the synthesis and properties of a series of self-assembled M_2L_4 complexes with variable amine groups, and the effect of these functionalities on the self-assembly process and optical properties of the system.[19]

RESULTS AND DISCUSSION

(1). Ligand Synthesis. The targeted ligand scaffold is shown in Figures 1 and 2, and has three components; a central substituted aniline core, acetylene spacers to provide complex size and 3-pyridyl groups at the termini for metal coordination.[20] Three types of ligands were synthesized to access complexes of varying interior cavity size and substitution. To incorporate functionality at different positions on the ligand (either endohedral, exohedral, or terminal), two different strategies were used

Received: May 23, 2011
Published: September 08, 2011

ACS Publications © 2011 American Chemical Society

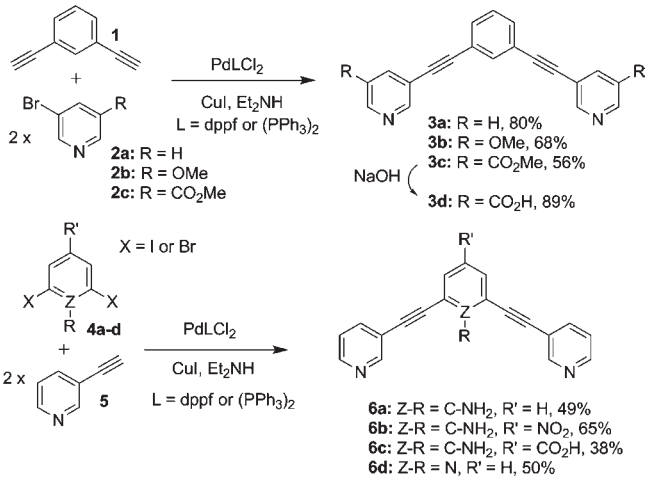

Figure 1. Synthesis of various ligands for complex formation.

(Figure 1). The unsubstituted ligand **3a** was synthesized by Sonogashira coupling[6f,21] of 1,3-diethynylbenzene **1** and 3-bromopyridine in good yield. Coupling with 5-substituted pyridines **2b** and **2c** allowed access to ligands with either electron rich or electron poor pyridines at the termini. Ligand **3c** was not suitable for complex formation because of insolubility, so the diester was hydrolyzed to diacid **3d** for further study.

Commercially available 2,6-dihaloarenes **4a**−**d** were used to access amine substitution at the central core. The challenge in creating endohedral amine substitution lies in metal-catalyzed derivatization of these aniline reactants. Fujita has shown that unreactive or protected species can be introverted in large $M_{12}L_{24}$ palladium-pyridine complexes,[15a−d] but amine functionalities are not innocent bystanders in metal-catalyzed coupling reactions: if they are not reactants (e.g., in Buchwald-Hartwig[22] coupling), they can react further with acetylene spacers to form indoles or other unwanted side products.[23] Double Sonogashira coupling of 3-ethynylpyridine **5** with unsubstituted 2,6-dihaloarenes is well-precedented, but the presence of an amino substituent in the 1 position requires careful control of conditions for optimized yields. The coupling conditions are remarkably similar to the conditions needed for indole synthesis from aminophenylacetylenes, and this was an especially problematic side reaction in the synthesis of **6a**. Protection of the amine **4a** as a carbamate or sulfonamide was ineffective, but use of $Pd(dppf)Cl_2$ as catalyst and careful control of temperature and the proportions of CuI and Pd allowed synthesis of **6a** in adequate yield. The presence of electron withdrawing groups on the central ring (**4b**−**d**) allowed coupling under milder conditions, and so competitive side reactions were minimized for the synthesis of **6b** and **6c**. The internal pyridine ligand **6d** was synthesized in moderate yield using the optimized conditions.

More conjugated, larger ligands were synthesized via a similar route, as shown in Figure 2. 1,3-Diethynylbenzene **1** was selectively coupled with 1,4-bromoiodobenzene **7** under Sonogashira conditions, and the resulting dibromide subjected to double Suzuki coupling with 3-pyridineboronic acid **9** to give the extended ligand **8**, albeit in poor yield. *Para*-bromophenylethynylpyridine **10**, accessed from 1,4-bromoiodobenzene and 3-ethynylpyridine (see Experimental Section) could be coupled to **1** to access the fully conjugated, longer ligand **11**. Attempts to display amines on the interior of these ligands have so far been unsuccessful.

(2). Self-Assembly and Complex Properties. Upon treatment with 0.5 mol-eq. $Pd(NO_3)_2$, or $PdOTf_2$, ligands **3**,**6**, **8**, and **11** all formed symmetrical self-assembled structures in DMSO solution, as determined by ^{1}H NMR spectroscopy. Molecular modeling suggests an M_2L_4 "paddle-wheel" complex, as shown in Figure 3.[24] Self-assembly of the ligands was studied by five methods: NMR, UV−vis absorption and fluorescence spectroscopy, mass spectrometry, and X-ray crystallography.

NMR Analysis. All species showed representative downfield chemical shifts due to coordination with the cationic Pd centers. The complexes are fully symmetric, and only one structure is observed in solution, irrespective of the ligand functionality. Figure 3 shows the ^{1}H NMR spectra for ligands **6a**, **6b**, and **3d**, and complexes $[(\mathbf{6a})_4\cdot\mathbf{Pd_2}](\mathbf{NO_3})_4$, $[(\mathbf{6b})_4\cdot\mathbf{Pd_2}](\mathbf{NO_3})_4$, and $[(\mathbf{3d})_4\cdot\mathbf{Pd_2}](\mathbf{NO_3})_4$ (see Supporting Information for all other spectra). Formation of the complex is extremely rapid, and occurs in less than 10 s at ambient temperature and millimolar concentration. Titration of $Pd(NO_3)_2$ into a dimethylsulfoxide (DMSO) solution of ligand shows that complete complex formation occurs upon addition of 0.5 mol equiv, indicating a 1:2 ratio of Pd: ligand in the self-assembled system (see Supporting Information). Introduction of functional groups has no effect on the coordination; neither the introverted amines (**6a**−**d**), carboxylic acids nor other pyridine nitrogens are competitive ligands for Pd, and are left uncoordinated in the final structure. As can be seen in Figures 3b and 3d, the NH_2 protons are visible for amine complexes $[(\mathbf{6a})_4\cdot\mathbf{Pd_2}](\mathbf{NO_3})_4$ and $[(\mathbf{6b})_4\cdot\mathbf{Pd_2}](\mathbf{NO_3})_4$ and have chemical shifts that are only slightly changed from those of the ligand. The most notable change in ^{1}H NMR is from protons H_a and H_b which show a downfield shift of >1 ppm. The other pyridine protons H_c and H_d are also shifted significantly downfield, but the protons on the central rings are only slightly changed because of their distance from the cationic Pd centers.

Even though the Pd centers are tetracationic, the complexes are stable to air, water, and light in both solution and the solid state for months. They are sensitive to competitive ligands for the Pd, however. Addition of stoichiometric amounts of salts such as hydroxide, carbonate, chloride, bromide, or iodide caused disruption of the complexes, forming ligand and PdX_2. Noncoordinating anions (SO_4^{2-}, BF_4^-, PF_6^-, SbF_6^-, NO_3^- or TfO^-) had no disruptive effect on the complexes. Slight changes in chemical shift were observed in complexes $[(\mathbf{6a})_4\cdot\mathbf{Pd_2}](\mathbf{NO_3})_4$ or $[(\mathbf{3a})_4\cdot\mathbf{Pd_2}](\mathbf{NO_3})_4$ upon addition of solutions of $NaSbF_6$ and $NaPF_6$, but these changes were minor, and no significant anion binding occurred in solution. The octahedral geometry of these anions should force four of the fluorides into coordination with the introverted amines in $[(\mathbf{6a})_4\cdot\mathbf{Pd_2}](\mathbf{NO_3})_4$, but molecular modeling suggests that the ions are too large for strong binding. The counterion had a considerable effect on the solubility of the complexes. The nitrate complexes were, without exception, only soluble in the presence of DMSO. They are insoluble in water, but an 80:20 mixture of water/DMSO is tolerated. No solubility is observed in less polar solvents, and the complexes can be precipitated from DMSO solution with addition of acetone. If $Pd(OTf)_2$ is used for the self-assembly, a greater range of solvents is possible. With the exception of $[(\mathbf{3d})_4\cdot\mathbf{Pd_2}](\mathbf{OTf})_4$, all complexes were soluble in either nitromethane or acetonitrile, and these solutions tolerated small amounts of less polar solvents such as toluene or chloroform. Interestingly, the complexes were

dx.doi.org/10.1021/ic201092s |*Inorg. Chem.* 2011, 50, 9430–9442

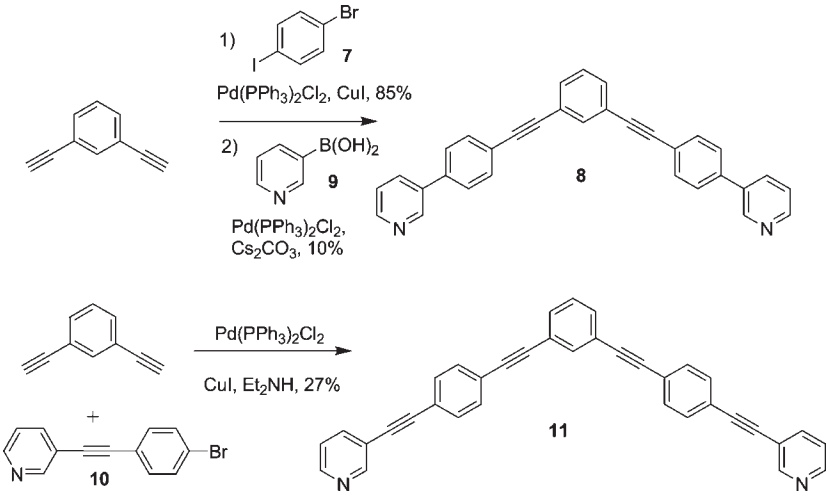

Figure 2. Synthesis of larger ligands for complex formation.

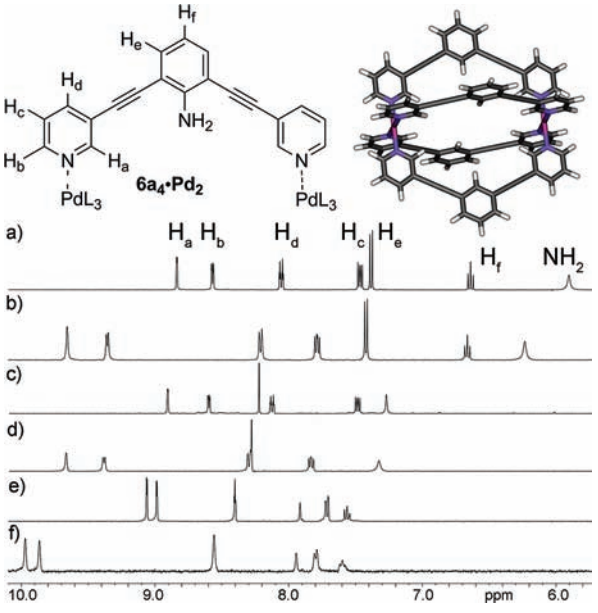

Figure 3. ^{1}H NMR spectra of representative ligands and complexes: (a) **6a**, (b) $[(\mathbf{6a})_4\cdot\mathbf{Pd}_2](\mathbf{NO}_3)_4$, (c) **6b**, (d) $[(\mathbf{6b})_4\cdot\mathbf{Pd}_2](\mathbf{NO}_3)_4$, (e) **3d**, (f) $[(\mathbf{3d})_4\cdot\mathbf{Pd}_2](\mathbf{NO}_3)_4$ (400 MHz, DMSO-d_6, 298K). Structure shown is a molecular model of $[(\mathbf{3a})_4\cdot\mathbf{Pd}_2](\mathbf{NO}_3)_4$ (SPARTAN, AM1 forcefield).

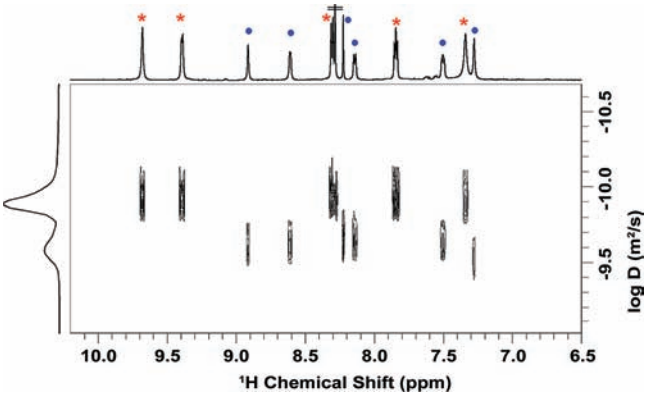

Figure 4. DOSY spectrum of a 1:1 mixture of **6b** and $[(\mathbf{6b})_4\cdot\mathbf{Pd}_2](\mathbf{NO}_3)_4$ (600 MHz, DMSO-d_6, 298 K, relaxation delay 2.5 s, diffusion delay 200 ms, gradient pulse length 2 ms). * = **6b**, • = $[(\mathbf{6b})_4\cdot\mathbf{Pd}_2](\mathbf{NO}_3)_4$.[27]

stable to acid; addition of 2% HNO_3 did not cause complex dissociation, even for amine complex $[(\mathbf{6b})_4\cdot\mathbf{Pd}_2](\mathbf{NO}_3)_4$. Other metals were tested for their coordination ability. Pt formed similar M_2L_4 complexes,[19] but no coordination was observed upon addition of various salts of Cu^I, Cu^{II}, Ni^{II}, Zn^{II}, Cd^{II}, Ag^I, or Au^I with noncoordinating counterions (BF_4^-, PF_6^-, NO_3^-, etc). The 3-pyridyl motif has free rotation, so could either be oriented "out", in a W-shaped conformation,[25] or "down" as shown in the Figures. No evidence of any other coordination patterns was observed for any of the ligands, indicating the stability of the M_2L_4 complex.

The complexes could be analyzed by diffusion NMR, as shown in Figure 4. A 1:1 mixture of ligand **6b** and complex $[(\mathbf{6b})_4\cdot\mathbf{Pd}_2](\mathbf{NO}_3)_4$ was subjected to DOSY analysis using the stimulated echo pulse sequence.[26] As expected, the larger complex diffused more slowly than the ligand: the diffusion constant for **6b** was $2.60 \pm 0.05 \times 10^{-10}$ m^2 s^{-1}, whereas the diffusion constant for $[(\mathbf{6b})_4\cdot\mathbf{Pd}_2](\mathbf{NO}_3)_4$ was $1.35 \pm 0.01 \times 10^{-10}$ m^2 s^{-1} (Figure 4). Diffusion constants were determined by curve fitting for the peaks at δ 8.92, 8.61 (**6b**) and δ 9.68, 9.39 ($[(\mathbf{6b})_4\cdot\mathbf{Pd}_2](\mathbf{NO}_3)_4$). The other peaks for the complex and ligand gave rise to similar diffusion constants (see Supporting Information).

To confirm the M_2L_4 structure of the complexes, mass spectral analysis was used. Because the nitrate complexes are only soluble in DMSO, the triflate complexes were used for MS analysis.[28] Either acetonitrile or nitromethane solutions of the complexes were subjected to electrospray mass spectrometry. The compounds were not completely stable to standard MS conditions, and low skimmer voltages were used to ensure that the $[M_2L_4\cdot OTf_3]^+$ could be seen. All of the complexes formed from addition of $Pd(OTf)_2$ to ligands **3a**−**b**, **6a**−**d**, and **8** could be analyzed by electrospray ionization mass spectrometry (ESI-MS). In each case signals for the singly positive complexes (having lost one triflate counterion) could be observed. The isotope patterns

dx.doi.org/10.1021/ic201092s |*Inorg. Chem.* 2011, 50, 9430–9442

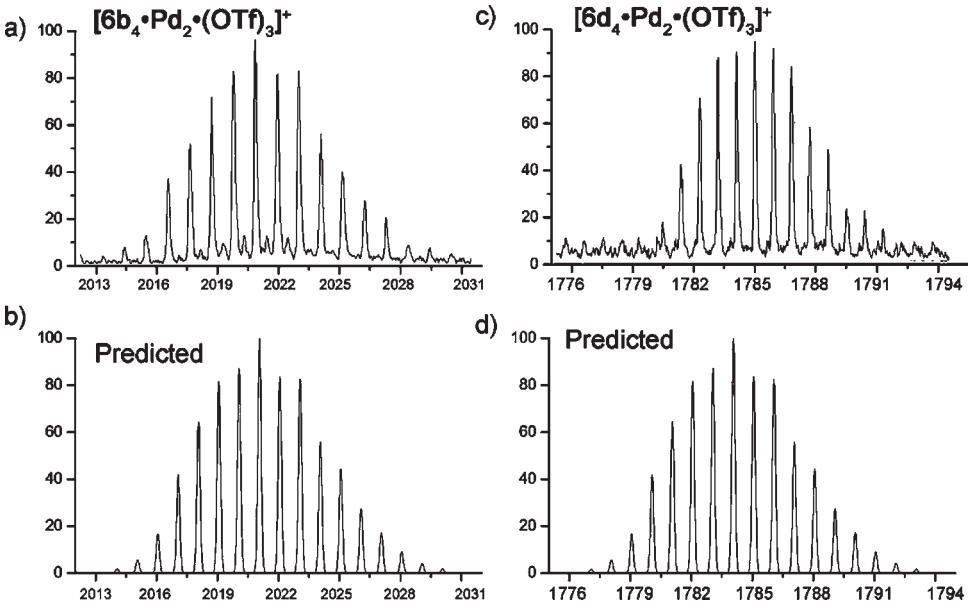

Figure 5. Observed and predicted regions of the M^+ region for complexes $[(\mathbf{6b})_4\cdot\mathbf{Pd}_2](\mathbf{OTf})_4$ and $[(\mathbf{6d})_4\cdot\mathbf{Pd}_2](\mathbf{OTf})_4$.

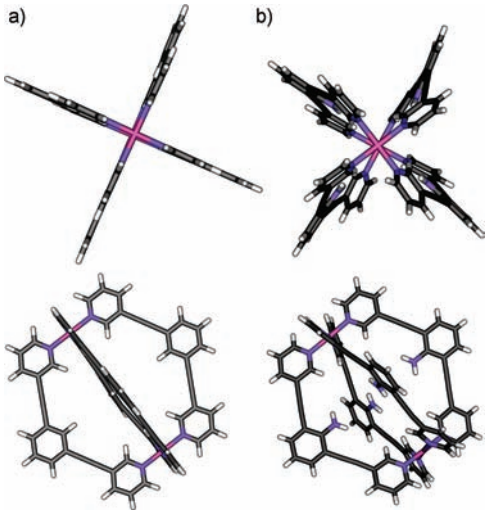

Figure 6. Comparison between the structures of (a) unfunctionalized $[(\mathbf{3a})_4\cdot\mathbf{Pd}_2](\mathbf{OTf})_4$ (ref 19) and (b) amine complex $[(\mathbf{6a})_4\cdot\mathbf{Pd}_2](\mathbf{OTf})_4$.

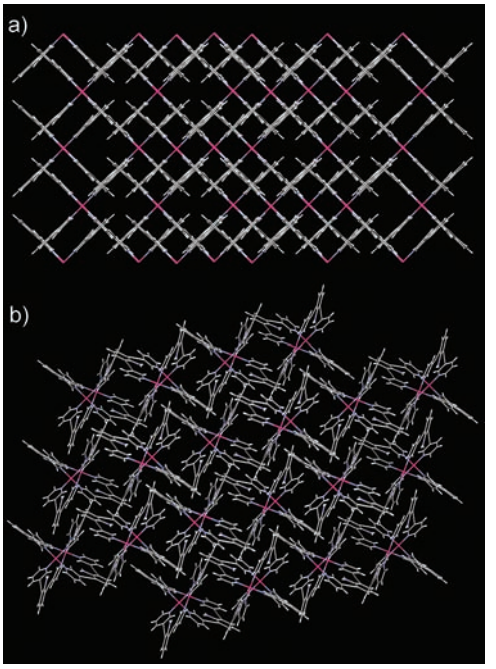

Figure 7. Comparison between the unit cells of (a) unfunctionalized $[(\mathbf{3a})_4\cdot\mathbf{Pd}_2](\mathbf{OTf})_4$ (ref 19) and (b) amine complex $[(\mathbf{6a})_4\cdot\mathbf{Pd}_2](\mathbf{OTf})_4$.

match the expected ratio for species with two Pd atoms present (see Experimental Section and Figure 5). Complexes $[(\mathbf{3d})_4\cdot\mathbf{Pd}_2](\mathbf{OTf})_4$ were not sufficiently soluble in MeCN or $MeNO_2$ for analysis, and $[\mathbf{11}_4\cdot\mathbf{Pd}_2](\mathbf{OTf})_4$ was too unstable for MS analysis. Only signals for $[M_2L_4\cdot OTf_2]^{2+}$ were observed for $[\mathbf{8}_4\cdot\mathbf{Pd}_2](\mathbf{OTf})_4$.

(3). X-ray Crystallographic Analysis. Crystallography of the endohedral complexes proved challenging. X-ray quality crystals of the unfunctionalized complex $[(\mathbf{3a})_4\cdot\mathbf{Pd}_2](\mathbf{OTf})_4$ could be obtained from slow evaporation of an acetonitrile solution of the complex.[19] X-ray diffraction analysis of this complex showed the formation of the predicted paddle-wheel form, with the interior cavity occupied by one disordered triflate molecule. Figures 6 and 7 show the structure; the complex is symmetrical and the ligands form a perfect "cross" at the Pd centers, with no bending or distortion. The space group was *Cm*, and as can be seen in Figure 7a, there are large cavities between the complexes, filled with disordered solvent molecules and triflate counterions. The distance between Pd atoms on adjacent complexes is 15.01 Å, and the aromatic rings of the ligand are completely offset, with no $\pi-\pi$ stacking or CH-π interactions observed.

Crystallization of the endohedrally substituted complexes was far less successful, and only the endohedral amine $[(\mathbf{6a})_4\cdot\mathbf{Pd}_2](\mathbf{OTf})_4$ was amenable to X-ray analysis. Crystals were grown by slow evaporation of an acetonitrile-toluene solution of $[(\mathbf{6a})_4\cdot\mathbf{Pd}_2](\mathbf{OTf})_4$, forming the structure seen in Figures 6b and 7b. The cationic complexes were well-resolved in the structure, but a significant amount of disorder was present in all the counterions and

dx.doi.org/10.1021/ic201092s |*Inorg. Chem.* 2011, 50, 9430–9442

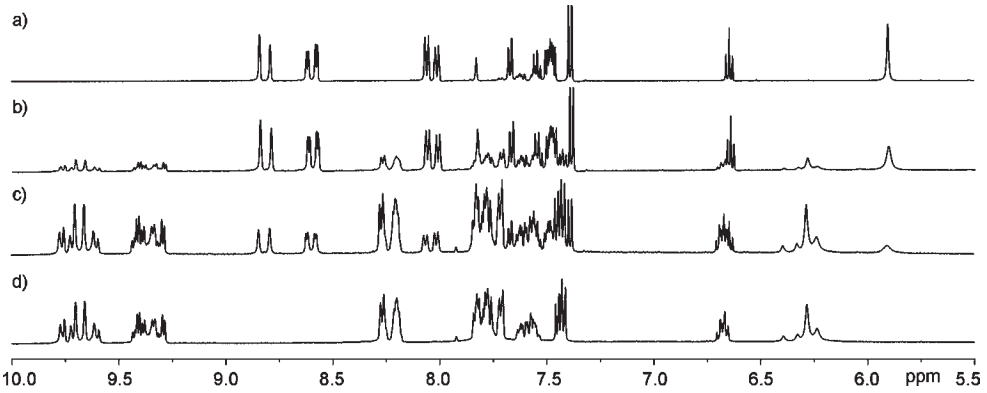

Figure 8. ^{1}H NMR spectra of the titration of $Pd(NO_3)_2$ into a 1:1 mixture of ligands **3a** and **6a** (7 mM, DMSO-d_6, 500 MHz, 298K). Molar equivalents $Pd(NO_3)_2$ (0.5 equiv of **3a**, 0.5 equiv of **6a**): (a) 0; (b) 0.16; (c) 0.32; (d) 0.50.

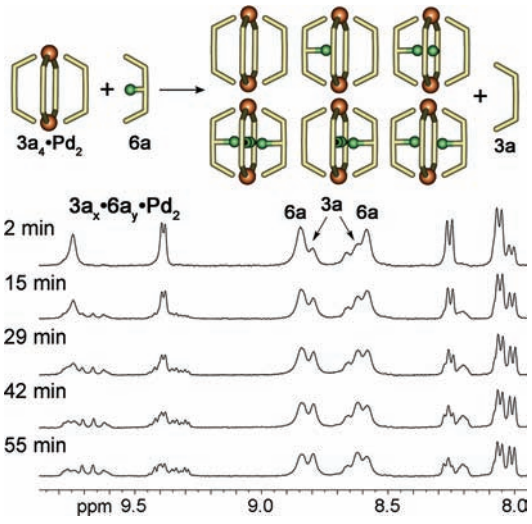

Figure 9. ^{1}H NMR spectra of the incorporation of ligand **6a** into of complex $[(\mathbf{3a})_4\cdot\mathbf{Pd_2}](\mathbf{NO_3})_4$ (400 MHz, DMSO-d_6, 14 mM, 300K).

solvent molecules; these are omitted from Figures 6 and 7 for clarity, but occupy the empty spaces in the structure. Interestingly, even though the only difference is the presence of *internal* amine groups, the solid state structure of $[(\mathbf{6a})_4\cdot\mathbf{Pd_2}](\mathbf{OTf})_4$ was markedly different from that of $[(\mathbf{3a})_4\cdot\mathbf{Pd_2}](\mathbf{OTf})_4$. This complex crystallizes in the $P\bar{1}$ space group, and shows significantly smaller cavities between complex molecules: the distance between Pd atoms on adjacent complexes is 11.70 Å. As in $[(\mathbf{3a})_4\cdot\mathbf{Pd_2}](\mathbf{OTf})_4$, there is a disordered triflate molecule present on the interior of the tetracationic complex. While the unfunctionalized complex $[(\mathbf{3a})_4\cdot\mathbf{Pd_2}](\mathbf{OTf})_4$ was cross-shaped and symmetric, the arms in $[(\mathbf{6a})_4\cdot\mathbf{Pd_2}](\mathbf{OTf})_4$ are twisted in the solid state structure. Solution-phase studies (vide infra) show that the formation of the tetramine complex $[(\mathbf{6a})_4\cdot\mathbf{Pd_2}](\mathbf{OTf})_4$ is almost as favorable as forming the unsubstituted complex $[(\mathbf{3a})_4\cdot\mathbf{Pd_2}](\mathbf{OTf})_4$.[29] Molecular modeling shows that the four endohedral amines can be accommodated in the interior cavity without unfavorable steric interactions between *each other*. While the exact cause of the altered crystal packing in $[(\mathbf{6a})_4\cdot\mathbf{Pd_2}](\mathbf{OTf})_4$ is not clear, the lack of interaction between the internal amine groups themselves suggests that interactions between these amine groups and the internally bound triflate anion have an effect on the structure.

In solution, solvent and anions exchange rapidly from the interior, but in the solid state one disordered triflate ion is forced to occupy the cavity interior. It is likely that this triflate anion has unfavorable interactions between the guest anion and the electron rich amines (interactions that are not present in $[(\mathbf{3a})_4\cdot\mathbf{Pd_2}](\mathbf{OTf})_4$). To allow its incorporation, the ligands twist out of plane, changing the host structure and crystal morphology, from monoclinic crystals in the *Cm* space group for $[(\mathbf{3a})_4\cdot\mathbf{Pd_2}](\mathbf{OTf})_4$ to triclinic crystals in the $P\bar{1}$ space group for $[(\mathbf{6a})_4\cdot\mathbf{Pd_2}](\mathbf{OTf})_4$. There are numerous CH-$\pi$ contacts between the individual $[(\mathbf{6a})_4\cdot\mathbf{Pd_2}](\mathbf{OTf})_4$ complexes, notably between H_d from the terminal pyridines (see Figure 3) and the central electron rich aniline ring. In addition, there are $\pi-\pi$ stacks between the central ring and the acetylene groups that are not observed in the $[(\mathbf{3a})_4\cdot\mathbf{Pd_2}](\mathbf{OTf})_4$ structure because of its offset nature.

(4). Ligand Dynamics. The synthesis of differentially functionalized ligands with similar geometries allows construction and analysis of unsymmetrical heterocomplexes. Analysis of self-assembled complexes with differentially functionalized ligands has to date been hindered by unsuitable NMR spectra; most published studies of ligand exchange behavior have relied upon mass spectrometric analysis alone as the NMR spectra are too complex or broad to allow accurate exchange analysis.[30]

All ligands **3**−**6** have pyridine groups for metal binding, and the coordination angle is identical for each. This allows analysis of the effect of different *electronics* on the self-assembly process, without significant change in metal−ligand geometry or steric interactions.[29] The well-defined NMR spectra in this system allow measurement of ligand exchange rate and heterocomplex composition by both ^{1}H NMR and ESI-MS. If two ligands are used, there are six products that can result - $\mathbf{A_4B_0}$, $\mathbf{A_3B_1}$, $\mathbf{A_2B_2}$, (two isomers - *cis* and *trans*), $\mathbf{A_1B_3}$ and $\mathbf{A_0B_4}$. To test the selectivity, $Pd(NO_3)_2$ was titrated into a 1:1 solution of **3a** and **6a** (Figure 8). A complex (but well-defined) ^{1}H NMR spectrum was observed that did not change over time. Interestingly, the incorporation of ligand into the complex with increasing [Pd] remained the same; both ligands **3a** and **6a** form complexes at the same rate, and the proportion of the heterocomplex mix is unchanged over time. In the case of **3a**/**6a**, the heterocomplex mixture is both the thermodynamic and kinetic product. From NMR and MS analysis (see Supporting Information), all six heterocomplexes can be observed in an approximately statistical

ratio. There is a slight bias toward incorporation of **3a** over **6a** in this case, but nothing substantial. The most useful region of the ^{1}H NMR spectrum for analysis is that corresponding to pyridine protons H_a and H_b (δ 9.0−10.0) as it is the least cluttered.

The sharp, distinguishable peaks for ligands and complexes in the same sample suggested that NMR techniques could be used to investigate the rate of ligand exchange. Unfortunately, the ligand exchange rate is too slow for measurement by 2D EXSY analysis of a mixture of ligand and corresponding homocomplex. The propensity for definable heterocomplex formation, however, allowed monitoring of the incorporation of a *different* ligand to a preformed complex over time by simple dynamic NMR measurements, as shown in Figure 9. Not all ligand combinations were amenable to this analysis, as significant overlap was present in the NMR spectra, making accurate integrations difficult. An equimolar amount of ligand **6a** was added to a preformed solution of complex $[(\mathbf{3a})_4\cdot\mathbf{Pd_2}](\mathbf{NO_3})_4$ and the decrease in [**6a**] was measured over time. The observed initial rates were calculated for ligand exchange, assuming that the rate of exchange of **6a** with **3a** is identical for each different heterocomplex ($[(\mathbf{3a})_4\cdot\mathbf{Pd_2}](\mathbf{NO_3})_4$, $[(\mathbf{3a})_3\cdot\mathbf{6a}\cdot\mathbf{Pd_2}](\mathbf{NO_3})_4$, $[(\mathbf{3a})_2\cdot(\mathbf{6a})_2\cdot\mathbf{Pd_2}](\mathbf{NO_3})_4$, $[\mathbf{3a}\cdot(\mathbf{6a})_3\cdot\mathbf{Pd_2}](\mathbf{NO_3})_4$). The fact that the different complexes are formed at the same rate lends credence to this assumption, and by measuring *initial* rates, the effect of different complex populations is minimized. Very little difference was observed between the exchange rate for incorporation of an electron rich ligand (aniline **6a**) than that for an electron-poor ligand (pyridine **6d**): $t_{1/2}$ (**6a:3a**) = 3.25 h, whereas $t_{1/2}$ (**6d:3a**) = 3.53 h. The variance in $t_{1/2}$ indicates that the ligand exchange process is not strongly dependent on external ligand concentration and type, but is consistent for the different ligands. Unfortunately, the complex NMR spectra preclude a more detailed mechanistic analysis. Diffusion NMR analysis of the $[(\mathbf{3a})_x\cdot(\mathbf{6a})_y\cdot\mathbf{Pd_2}](\mathbf{NO_3})_4$ heterocomplex mix was unsuccessful in distinguishing the individual complexes (see Supporting Information).

Heterocomplex formation also allows NOE analysis of the complexes. Obviously no NOE contacts are visible between protons that are close in space for the symmetrical homocomplexes such as $[(\mathbf{3a})_4\cdot\mathbf{Pd_2}](\mathbf{NO_3})_4$, but once the ligands are desymmetrized, NOESY spectra can be used to analyze the self-assembled product. The most useful heterocomplex mix is $[\mathbf{6a}_{(x)}\cdot\mathbf{6d}_{(y)}\cdot\mathbf{Pd_2}](\mathbf{NO_3})_2$, as the different signals for H_a are distinguished in the ^{1}H NMR spectrum (see Figure 10). Varying the proportions of ligands **6a** and **6d** ligand concentrations allowed assignment of the different resonances. When a 1:1 ratio of ligands is used, NOE contacts can be observed between protons H_a on adjacent ligands in the complex. The H_a peaks from $[(\mathbf{6a})_3\cdot\mathbf{6d}\cdot\mathbf{Pd_2}](\mathbf{NO_3})_4$ (δ 9.97, 9.70, and 9.58) show NOE crosspeaks between each other, as do the H_a peaks from $[(\mathbf{6a})_2\cdot(\mathbf{6d})_2\cdot\mathbf{Pd_2}](\mathbf{NO_3})_4$ (δ 9.85 and 9.63), but no crosspeaks can be seen from $[(\mathbf{6a})_4\cdot\mathbf{Pd_2}](\mathbf{NO_3})_4$ (δ 9.66) to anything else. No peaks are visible in the ^{1}H spectrum for the $[(\mathbf{6d})_4\cdot\mathbf{Pd_2}](\mathbf{NO_3})_4$ complex, and any peaks from $[(\mathbf{6a})\cdot(\mathbf{6d})_3\cdot\mathbf{Pd_2}](\mathbf{NO_3})_4$ are small and overlap with the other resonances. No other interligand NOE signals are visible (although the different H_b peaks are poorly differentiated in the ^{1}H NMR spectrum). The mass spectrum of the system is consistent with this preferential incorporation; only four heterocomplexes are observed, $[(\mathbf{6d})_4\cdot\mathbf{Pd_2}](\mathbf{OTf})_4$ is not seen at all and the signal for $[\mathbf{6a}\cdot(\mathbf{6d})_3\cdot\mathbf{Pd_2}](\mathbf{OTf})_4$ is weak.

The formation of heterocomplexes between the other synthesized ligands was investigated by ^{1}H NMR spectra in an attempt

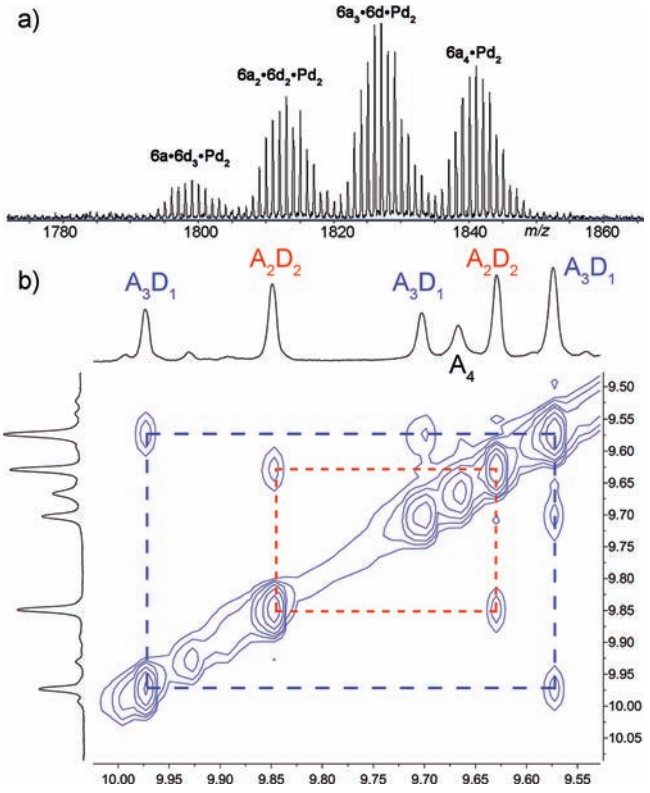

Figure 10. Analysis of the $\mathbf{6a}_{(x)}\cdot\mathbf{6d}_{(y)}\cdot\mathbf{Pd_2}$ heterocomplex system. (a) ESI-MS spectrum of $[\mathbf{6a}_{(x)}\cdot(\mathbf{6d})_{(y)}\cdot\mathbf{Pd_2}](\mathbf{OTf})_4$; (b) Downfield region of the 2D NOESY spectrum of $[\mathbf{6a}_{(x)}\cdot\mathbf{6d}_{(y)}\cdot\mathbf{Pd_2}](\mathbf{NO_3})_4$, indicating crosspeaks between H_a resonances on adjacent ligands (500 MHz, DMSO-d_6, 298 K).

to identify ligand combinations that would show self-sorting behavior. Unfortunately, while all the ligands tested proved suitable for heterocomplex formation, NMR spectra showed statistical mixtures of products with only slight preference for one complex over the others. The greatest bias was observed for the $[\mathbf{6a}_{(x)}\cdot\mathbf{6d}_{(y)}\cdot\mathbf{Pd_2}](\mathbf{NO_3})_4$ system shown above. The preferential incorporation of amine ligand **6a** over pyridine ligand **6d** suggested that electron-rich ligands were more effective for complex formation, but this phenomenon was not observed for terminal methoxy ligand **3b**, and no obvious pattern could be observed in the self-assembly. This is not surprising, as the difference in donor ability for the ligands **3a**−**d** and **6a**−**d** is small. If the elongated ligands **8** and **11** were mixed with the smaller ligands **3**/**6**, no mixing was observed, and only homocomplexes were observed. This is consistent with the fact that no other coordination geometries than the paddle-wheel are observed: the M_2L_4 structure is the most favorable, and the longer ligands do not mix with their smaller counterparts, a process that would require a less favorable complex geometry.

The lack of any strong preference between the small ligands provides an interesting counterpart to the solid state structure of $[(\mathbf{6a})_4\cdot\mathbf{Pd_2}](\mathbf{OTf})_4$. The complex with endohedral amines was far less stable in the solid state than the unfunctionalized **3a**, presumably because of repulsive interactions between the amines and the triflate ion in the cavity. These interactions forced the complex from the cross-shaped ideal geometry into a twisted form. In solution, that appears not to be the case: while the exact geometry of the $[(\mathbf{6a})_4\cdot\mathbf{Pd_2}](\mathbf{OTf})_4$ complex is unknown,

dx.doi.org/10.1021/ic201092s |*Inorg. Chem.* 2011, 50, 9430–9442

Table 1. UV-Vis Absorbance and Fluorescence Emission Characteristics of the Pd_2L_4 Complexes

entry	name	ε ($cm^{-1}\cdot M^{-1}$)[a]	λ_{max}(abs) (nm)	excited @	λ_{max}(emis) (nm)	Φ (%)
1	CH complex $[\mathbf{3a}_4\cdot Pd_2](NO_3)_4$	1.20×10^5	286, 305	305	359, 378	<0.2
	ligand **3a**	1.11×10^5	287, 305	305	359, 376	<0.2
2	diacid complex $[\mathbf{3d}_4\cdot Pd_2](NO_3)_4$	4.57×10^4	288	288	429	<0.2
	ligand **3d**	4.40×10^4	288	288	437	<0.2
3	dimethoxy complex $[\mathbf{3b}_4\cdot Pd_2](NO_3)_2$	4.15×10^4	287, 313	313	356	0.41
	ligand **3b**	4.06×10^4	287, 313	313	355	0.44
4	aniline complex $[\mathbf{6a}_4\cdot Pd_2](NO_3)_4$	1.43×10^5	280, 328, 374	374	441	44
	ligand **6a**	1.32×10^5	281, 331, 374	374	441	36
5	nitroaniline complex $[\mathbf{6b}_4\cdot Pd_2](NO_3)_4$	3.64×10^4	267, 387	387	445	0.27
	ligand **6b**	3.33×10^4	266, 388	387	449	<0.2
6	Acid-aniline complex $[\mathbf{6c}_4\cdot Pd_2](NO_3)_4$	4.80×10^4	281, 380	380	426	83
	ligand **6c**	4.44×10^4	281, 381	380	426	87
7	pyridine complex $[\mathbf{6d}_4\cdot Pd_2](NO_3)_4$	5.64×10^4	271, 319	319	349	1.1
	ligand **6d**	5.17×10^4	269, 324	319	349	1.1
8	elongated complex $[\mathbf{8}_4\cdot Pd_2](NO_3)_4$	6.23×10^4	309	309	344, 361	21
	ligand **8**	6.00×10^4	309	309	344, 361	23
9	elongated complex $[\mathbf{11}_4\cdot Pd_2](NO_3)_4$	7.17×10^3	311,475	311	354, 371, 381	10
	ligand **11**	3.69×10^3	325	325	354, 371	38

[a] ε_{max} is quoted for the absorption at lowest wavelength.

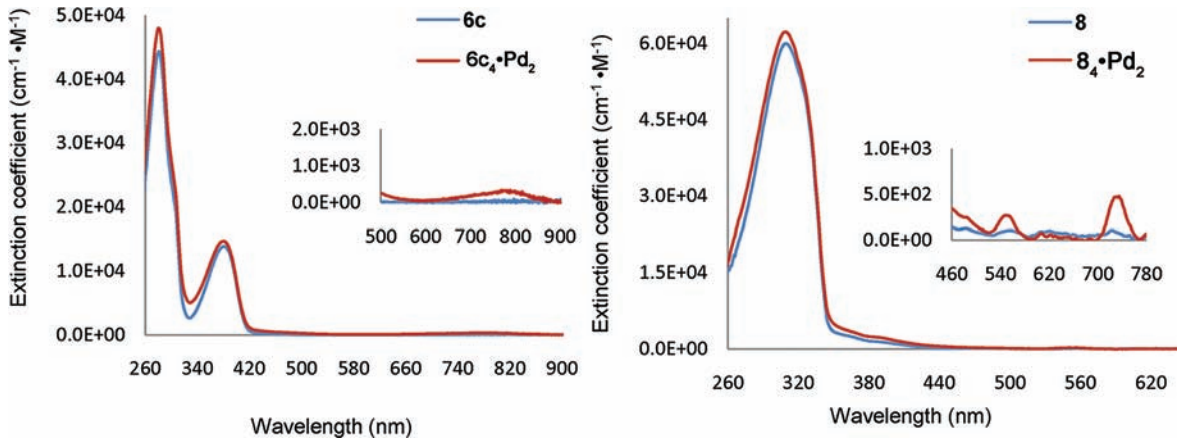

Figure 11. Absorption spectra in DMSO solution for ligands **6c** and **8**, and complexes $[(\mathbf{6c})_4\cdot Pd_2](NO_3)_4$ and $[\mathbf{8}_4\cdot Pd_2](NO_3)_4$, showing weak high energy MLCT peaks for the complexes.

formation of the complex is no less favorable than for any other ligand with no endohedral substituents. This (along with the lack of NMR evidence for anion binding) suggests that the triflate or nitrate counterions are not present in the complex cavity in solution, rather that the DMSO solvent occupies the cavity interior, giving rise to different complex stabilities in the solution phase and the solid state.

(5). Optical Properties. The highly conjugated nature of the ligands and complexes allows analysis of their optical properties. All of the complexes described show strong UV−vis absorption spectra, as shown in Table 1. The absorption spectra are dominated by ligand-based $\pi-\pi^*$ transitions, indicating that the complexes are mainly Werner-type complexes with little electron density residing on the metal centers, as would be expected from the high charge. To eliminate any possibility of ligand dissociation at the low concentrations used, the UV−vis absorption spectrum of the Pd complexes were recorded at varying concentrations up to 0.35×10^{-7} M, and their spectral features were found to be identical to those recorded in more concentrated solution (2.2×10^{-5} M). We can therefore conclude that the Pd complexes did not undergo dissociation at very low concentrations in DMSO.

The greatest variance in absorbance between ligand and complex was an increased extinction coefficient for the complex, along with small hypsochromic shifts from (1−14 nm). Only the pyridine ligand **6d** exhibited a bathochromic shift of 2 nm upon complexation. These differences are consistent with other Pd−N complexes in the literature.[31] For example, a 1.1-fold increase in extinction coefficient and a hypsochromic shift of 1 nm was observed between aniline ligand **6a** and the corresponding complex for the absorbance maximum at 281 nm. At the 331 nm absorbance

dx.doi.org/10.1021/ic201092s |Inorg. Chem. 2011, 50, 9430–9442

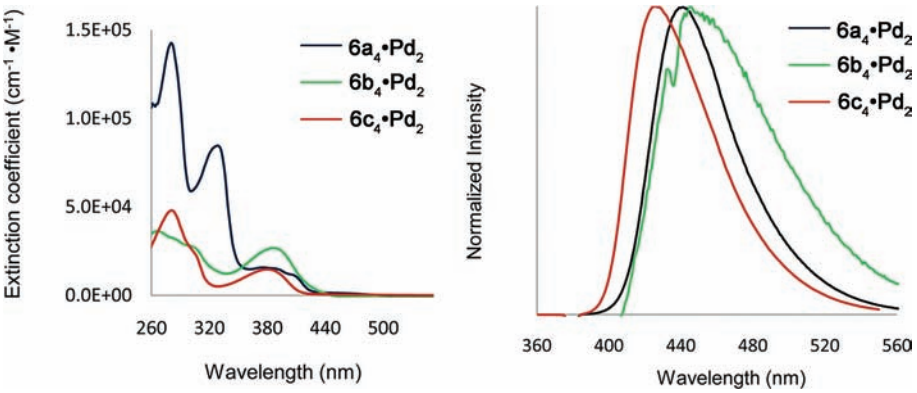

Figure 12. Absorption/emission spectra for DMSO solutions of amine-containing complexes $[(\mathbf{6a})_4\cdot\mathbf{Pd}_2](\mathbf{NO}_3)_4$, $[(\mathbf{6b})_4\cdot\mathbf{Pd}_2](\mathbf{NO}_3)_4$, and $[(\mathbf{6c})_4\cdot\mathbf{Pd}_2](\mathbf{NO}_3)_4$.

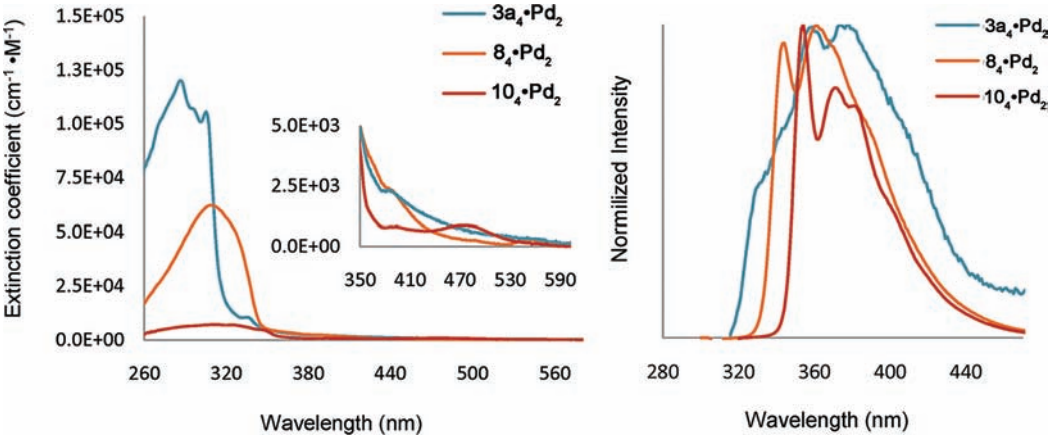

Figure 13. Absorption/emission spectra for DMSO solutions of complex $[(\mathbf{3a})_4\cdot\mathbf{Pd}_2](\mathbf{NO}_3)_4$ and elongated complexes $[(\mathbf{6a})_4\cdot\mathbf{Pd}_2](\mathbf{NO}_3)_4$, $[\mathbf{8}_4\cdot\mathbf{Pd}_2](\mathbf{NO}_3)_4$, and $[\mathbf{11}_4\cdot\mathbf{Pd}_2](\mathbf{NO}_3)_4$.

maximum, the opposite was observed; a 1.5-fold reduction in extinction coefficient was recorded and a 3 nm hypsochromic shift. Metal−ligand charge transfer transitions were generally weak, but they were observed for a number of the complexes. The transitions had low ε values ($\sim 10^2$−10^3 cm^{-1} M^{-1}) and were observed most notably for extended complex $[\mathbf{8}_4\cdot\mathbf{Pd}_2](\mathbf{NO}_3)_4$ and amino acid complex $[(\mathbf{6c})_4\cdot\mathbf{Pd}_2](\mathbf{NO}_3)_4$ (Figure 11).

Fluorescence emission spectra were also recorded, and the quantum yields for the fluorescent complexes established. The quantum yields varied significantly for the various complexes, from very low values (<0.2% for diacid complex $[(\mathbf{3d})_4\cdot\mathbf{Pd}_2](\mathbf{NO}_3)_4$) to high yields (83% for amino acid complex $[(\mathbf{6c})_4\cdot\mathbf{Pd}_2](\mathbf{NO}_3)_4$). These variations will be discussed below. Stokes' shifts also varied; the average shift was on the order of 70 nm, but this varied from 30 nm for pyridine complex $[(\mathbf{6d})_4\cdot\mathbf{Pd}_2](\mathbf{NO}_3)_4$ to 141 nm for diacid complex $[(\mathbf{3d})_4\cdot\mathbf{Pd}_2](\mathbf{NO}_3)_4$. The presence of heavy metals did not cause significant quenching of the fluorescence, and an increase in Φ was observed for aniline complex $[(\mathbf{6a})_4\cdot\mathbf{Pd}_2](\mathbf{NO}_3)_4$.

(a). Amine-Functionalized Complexes. The absorption spectrum for the aniline complexes $[(\mathbf{6a})_4\cdot\mathbf{Pd}_2](\mathbf{NO}_3)_4$−$[(\mathbf{6c})_4\cdot\mathbf{Pd}_2](\mathbf{NO}_3)_4$ is shown in Figure 12. The aniline complex $[(\mathbf{6a})_4\cdot\mathbf{Pd}_2](\mathbf{NO}_3)_4$ was strongly absorbing, with a molar extinction coefficient of 1.43×10^5 M^{-1} cm^{-1}. Three absorption peaks were observed at 280, 328, and 374 nm. Several variations in the absorption spectra were observed in the presence of extroverted electron withdrawing groups. The moderately electron withdrawing group in acid-aniline complex $[(\mathbf{6c})_4\cdot\mathbf{Pd}_2](\mathbf{NO}_3)_4$ resulted in a 3-fold decrease in absorption with respect to $[(\mathbf{6a})_4\cdot\mathbf{Pd}_2](\mathbf{NO}_3)_4$ as well as a hypsochromic shift of 6 nm for the absorbance at longest wavelength. Stronger acceptors such as nitroaniline $[(\mathbf{6c})_4\cdot\mathbf{Pd}_2](\mathbf{NO}_3)_4$ resulted in 4-fold decrease in absorption and a bathochromic shift of 13 nm.

All three complexes gave emission spectra, as shown in Figure 12b. The Stokes' shift of these complexes varied strongly with substitution, with aniline complex $[(\mathbf{6a})_4\cdot\mathbf{Pd}_2](\mathbf{NO}_3)_4$ giving a 113 nm shift. The presence of electron withdrawing groups on the ring reduced the shift, with a 58 nm Stokes' shift observed for the strongly withdrawn nitroaniline complex $[(\mathbf{6b})_4\cdot\mathbf{Pd}_2](\mathbf{NO}_3)_4$. These complexes were strongly fluorescent, with quantum yields varying between 44 and 83%. The presence of the nitro group in $[(\mathbf{6b})_4\cdot\mathbf{Pd}_2](\mathbf{NO}_3)_4$ caused significant fluorescence quenching, with $\Phi < 0.2\%$.

(b). Terminally Functionalized Complexes. The amine functionality was essential for strong fluorescence in the smaller complexes. The parent CH complex was only weakly fluorescent, with $\Phi < 0.2\%$. Incorporation of electron donors and acceptors to the terminal pyridine groups had little effect, although the quantum yield for dimethoxy complex $[(\mathbf{3b})_4\cdot\mathbf{Pd}_2](\mathbf{NO}_3)_4$ was more than double that of $[(\mathbf{3a})_4\cdot\mathbf{Pd}_2](\mathbf{NO}_3)_4$, with $\Phi = 0.41\%$.

dx.doi.org/10.1021/ic201092s |*Inorg. Chem.* 2011, 50, 9430–9442

The emission spectrum for $[(\mathbf{3a})_4\cdot\mathbf{Pd_2}](\mathbf{NO_3})_4$ is broad, with two maxima at 359 and 378 nm, whereas the emission spectra of $[(\mathbf{3b})_4\cdot\mathbf{Pd_2}](\mathbf{NO_3})_4$ and $[(\mathbf{3d})_4\cdot\mathbf{Pd_2}](\mathbf{NO_3})_4$ are less structured (see Supporting Information). A hypsochromic shift is noticed for the dimethoxy emission spectrum with λ_{max} = 356 nm. On the other hand, there is a noticeable bathochromic shift observed for the extroverted acid complex corresponding to the peak at λ_{max} = 429 nm.

(c). Elongated Complexes. Increasing the conjugation of the ligands caused slight changes in the absorption spectra; a bathochromic shift of 4 nm was observed between the lowest energy absorptions of complexes $[(\mathbf{3a})_4\cdot\mathbf{Pd_2}](\mathbf{NO_3})_4$ and $[\mathbf{8_4}\cdot\mathbf{Pd_2}](\mathbf{NO_3})_4$ (Figure 13). A bathochromic shift of 6 nm was observed between $[(\mathbf{3a})_4\cdot\mathbf{Pd_2}](\mathbf{NO_3})_4$ and the largest complex $[\mathbf{11_4}\cdot\mathbf{Pd_2}](\mathbf{NO_3})_4$. Elongation reduces the absorption efficiency, though, as the molar extinction coefficient of $[(\mathbf{3a})_4\cdot\mathbf{Pd_2}](\mathbf{NO_3})_4$ was $1.2 \times 10^5\ M^{-1}\ cm^{-1}$, whereas $[\mathbf{8_4}\cdot\mathbf{Pd_2}](\mathbf{NO_3})_4$ showed a 2-fold decrease in ε. A 17-fold decrease in ε was observed for the $\pi-\pi^*$ intraligand transition of $[\mathbf{11_4}\cdot\mathbf{Pd_2}](\mathbf{NO_3})_4$, but this system did show a metal-to-ligand charge-transfer transition at 475 nm. The emission spectra of $[\mathbf{8_4}\cdot\mathbf{Pd_2}](\mathbf{NO_3})_4$, and $[\mathbf{11_4}\cdot\mathbf{Pd_2}](\mathbf{NO_3})_4$ are more highly structured than the absorption spectra, which is devoid of structure. The more conjugated, longer ligands also show more efficient fluorescence than their shorter counterparts, with Φ = 21% and 10% for $[\mathbf{8_4}\cdot\mathbf{Pd_2}](\mathbf{NO_3})_4$, and $[\mathbf{11_4}\cdot\mathbf{Pd_2}](\mathbf{NO_3})_4$, respectively.

CONCLUSIONS

In conclusion, a series of tetracationic M_2L_4 palladium-pyridyl paddle-wheel complexes have been synthesized with different appended functionalities including endohedral amines and exohedral carboxylic acids. The metal−ligand coordination occurs solely at the terminal pyridines, even in the presence of amine or other pyridine groups, and the M_2L_4 structure is favored, with no polymeric aggregates observed. Structural analysis is possible using NMR techniques (including Diffusion NMR and 2D NOESY), mass spectrometry, and X-ray crystallography. The solid state analysis shows a large change in crystal morphology upon introduction of the endohedral amine groups, because of a twisting of the ligands in the paddle-wheel complex with respect to the unfunctionalized system. This twisting leads to a far more closely packed structure that takes advantage of $\pi-\pi$ stacking and CH-π interactions, something not observed in the unfunctionalized system, which shows large cavities and highly offset crystal packing.

Combination of different ligands allows analysis of the self-assembly properties of the system; both electron rich and electron poor ligands exchange with a half-life of ~3 h. The different donor properties of the functionalized ligands give rise to biased heterocomplex formation, with favorability observed for self-assembly of endohedral amines over pyridyl substrates. The most efficient fluorescence belongs to complexes with endohedral amines, giving quantum yields of up to 83%. The construction of larger ligands is possible, and these more conjugated complexes also show good fluorescence properties. Further research on the properties of endohedrally functionalized complexes is underway in our laboratory.

EXPERIMENTAL SECTION

General Information. ^{1}H and ^{13}C NMR spectra were recorded on either a Varian Inova 400 or 500 spectrometer. 2D NOESY spectra were recorded on a Varian Inova 500 spectrometer, using the pulse sequence supplied with the Varian operating system. DOSY spectra were recorded on a Bruker Avance 600 spectrometer. Proton (^{1}H) chemical shifts are reported in parts per million (δ) with respect to tetramethylsilane ($Si(CH_3)_4$, δ = 0), and referenced internally with respect to the protio solvent impurity. Carbon (^{13}C) chemical shifts are reported in parts per million (δ) with respect to tetramethylsilane ($Si(CH_3)_4$, δ = 0), and referenced internally with respect to the solvent ^{13}C signal (either $CDCl_3$ or DMSO-d_6). Deuterated NMR solvents were obtained from Cambridge Isotope Laboratories, Inc., Andover, MA, and used without further purification. Mass spectra were recorded on an Agilent 6210 LC TOF mass spectrometer using electrospray ionization and processed with an Agilent MassHunter Operating System. The complexes were diluted to concentrations of ~50 μM. Gentle source conditions were employed to keep the metal−ligand complexes intact. This was achieved by lowering voltages in the capillary/skimmer interface region. UV−vis absorption spectra were recorded on a Varian Cary 50 UV−visible spectrophotometer. The absorption spectra of the free ligands and their corresponding metal complexes were recorded in solution at room temperature. Steady-state fluorescence measurements were obtained using a Spex Fluorolog-Tau3 fluorescence spectrophotometer and recorded at 1 nm increments and 1 s integration time. The fluorescence emission and excitation spectra of the free ligands and their corresponding metal complexes were recorded in diluted solutions. Optical data was recorded in standard 10 mm path length Spectrosil Far UV quartz cuvettes. Molecules and reagents for ligand/complex synthesis were obtained from Aldrich Chemical Co., St. Louis, MO, and were used as received. Solvents were dried through a commercial solvent purification system (SG Water, Inc.). $Pd(OTf)_2$ was synthesized according to literature procedures.[32] The synthesis of ligand **3a** and complex $[(\mathbf{3a})_4\cdot\mathbf{Pd_2}](\mathbf{NO_3})_4$, including crystallographic analysis are described in ref 19. Molecular modeling (semiempirical calculations) was performed using the AM1 force field using SPARTAN.[33]

EXPERIMENTAL PROCEDURES

General Procedure for Complex Formation. The mixture of ligand (0.1 mmol) and $Pd(NO_3)_2\cdot xH_2O$ (0.05 mmol) in DMSO (2 mL) was stirred at room temperature for 30 min, then precipitated by addition of acetone and hexane. The precipitate was washed carefully with acetone (6 mL) and dried under vacuum to yield the solid product.

1,3-Bis((5-methoxypyridin-3-yl)ethynyl)benzene ***3b***. To a 10 mL round-bottomed flask equipped with stir bar and reflux condenser was added 1,3-diethynylbenzene (48 mg, 0.376 mmol), 3-bromo-5-methoxypyridine (178 mg, 0.946 mmol), 1,1′ bis(diphenylphosphino)ferrocene palladium(II) dichloride (15.3 mg, 0.019 mmol), and copper(I) iodide (4 mg, 0.022 mmol). The mixture was placed under nitrogen, and degassed diisopropylamine (1 mL) was added. The reaction was heated at 80 °C for 22 h. Ethyl acetate (10 mL) was added, the reaction filtered, and the filtrate evaporated under reduced pressure. The crude product was recrystallized from ethyl acetate to yield a brown solid (87 mg, 68%). ^{1}H NMR (400 MHz, DMSO-d_6) δ 8.37 (s, 2H); 8.33 (d, J = 2.0 Hz, 2H); 7.81 (s, 1H); 7.66 (dd, J = 1.2, 8.4 Hz, 2H); 7.60 (dd, J = 2.0, 2.8 Hz; 2H); 7.54 (t, J = 7.7 Hz, 1H); 3.87 (s, 6H); ^{13}C NMR (100 MHz, DMSO-d_6) δ 154.9; 143.8; 138.15; 134.3; 132.0; 129.6; 122.4; 122.1; 119.4; 90.9; 87.0; 55.7; HRMS (ESI) m/z: calcd for $C_{22}H_{17}N_2O_2$ $(M+H)^+$ 341.1285; found 341.1295.

Complex $[(\mathbf{3b})_4\cdot Pd_2](NO_3)_4$. ^{1}H NMR (400 MHz, DMSO-d_6) δ 9.36 (s, 2H); 9.13 (d, J = 2.4 Hz, 2H); 7.92 (s, 1H); 7.91 (s, 2H); 7.70 (d, J = 8.4 Hz, 2H); 7.59 (t, J = 7.6 Hz, 1H); 3.97 (s, 6H); ^{13}C NMR (100 MHz, DMSO-d_6) δ 156.7; 144.4; 139.3; 134.2; 133.3; 130.0; 126.7; 122.3; 121.7; 93.5; 85.0; 56.8; HRMS (ESI) m/z: calcd for $C_{91}H_{64}N_{12}O_9F_9S_3{}^{106}Pd^{108}Pd$ $(M - OTf^-)^+$ 2021.1476; found 2021.1514.

dx.doi.org/10.1021/ic201092s |*Inorg. Chem.* 2011, 50, 9430–9442

Dimethyl 5,5′-(1,3-phenylenebis(ethyne-2,1-diyl))dinicotinate ***3c***. To a 10 mL round-bottomed flask equipped with stir bar and reflux condenser was added 1,3-diethynylbenzene (25 mg, 0.198 mmol), methyl 5-bromonicotinate (86.6 mg, 0.401 mmol), and 1,1′ bis(diphenylphosphino)ferrocene palladium(II) dichloride (8.4 mg, 0.010 mmol. The mixture was placed under nitrogen and anhydrous *N*,*N*′-dimethylformamide (1 mL), and degassed triethylamine (0.5 mL) was added. The reaction was heated at 80 °C for 16 h. Water (10 mL) was added, and the resultant precipitate filtered. The crude product was purified by flash column chromatography on silica gel (CH_2Cl_2) to yield a tan solid (44 mg, 56%). ^{1}H NMR (400 MHz, $CDCl_3$) δ 9.15 (d, J = 1.6 Hz, 2H); 8.90 (d, J = 1.6 Hz, 2H); 8.41 (t, J = 2.0 Hz, 2H); 7.76 (s, 1H); 7.56 (dd, J = 1.6, 7.6 Hz, 2H); 7.40 (t, J = 7.6 Hz, 1H); 3.98 (s, 6H); ^{13}C NMR (100 MHz, $CDCl_3$) δ 165.22 155.6; 149.7; 139.5; 135.0; 132.3; 128.9; 125.8; 122.9; 120.3; 92.6; 85.9; 52.8; HRMS (ESI) m/z: calcd for 397.1183; found 397.1154.

5,5′-(1,3-Phenylenebis(ethyne-2,1-diyl))dinicotinic acid ***3d***. To a 10 mL round-bottom flask equipped with stir bar and reflux condenser was added dimethyl 5,5′-(1,3-phenylenebis(ethyne-2,1-diyl))dinicotinate (64 mg, 0.162 mmol), sodium hydroxide (53 mg, 1.32 mmol), tetrahydrofuran (0.8 mL), and water (0.2 mL). The reaction was heated at 65 °C for 16 h. The reaction was allowed to cool, and 10% aq HCl was added until acidic.The resultant precipitate was filtered to yield a tan solid (53 mg, 89%). ^{1}H NMR (400 MHz, DMSO-d_6) δ 13.68 (br s, 2H); 9.06 (d, J = 2.0 Hz, 2H); 8.99 (d, J = 1.6 Hz, 2H); 8.40 (t, J = 2.0 Hz, 2H); 7.91 (s, 1H); 7.71 (dd, J = 1.2, 7.6 Hz, 2H); 7.56 (t, J = 7.6 Hz, 1H); ^{13}C NMR (100 MHz, DMSO-d_6) δ 165.5; 154.9; 149.5; 139.1; 134.6; 132.3; 129.6; 126.5; 122.2; 119.2; 92.0; 86.1; HRMS (ESI) m/z: calcd for 369.0870; found 369.0861.

Complex [(3d)$_4$·Pd$_2$](NO$_3$)$_4$. ^{1}H NMR (400 MHz, DMSO-d_6) δ 9.98 (d, J = 1.2 Hz, 2H); 9.87 (d, J = 1.6 Hz, 2H); 8.561 (s, 2H); 7.942 (s, 1H); 7.80 (dd, J = 1.2, 8.0 Hz, 2H); 7.60 (t, J = 8.0 Hz, 1H); ^{13}C NMR (100 MHz, DMSO-d_6) δ 163.8; 155.8; 151.3; 142.5; 134.1; 133.7; 130.1; 128.5; 122.4; 121.7; 94.5; 84.9. HRMS data could not be obtained because of solubility issues.

2,6-Bis(pyridin-3-ylethynyl)aniline ***6a***. To a 10 mL round-bottomed flask equipped with stir bar and reflux condenser was added 2,6-dibromoaniline (129.8 mg, 0.517 mmol), 3-ethynylpyridine (129.2 mg, 1.253 mmol), 1,1′ bis(diphenylphosphino)ferrocene palladium(II) dichloride (21.6 mg, 0.026 mmol), and copper(I) iodide (5.6 mg, 0.029 mmol). The mixture was placed under nitrogen and dry, degassed tetrahydrofuran (THF, 2 mL) and degassed diisopropylamine (2 mL) were added. The reaction was heated at 80 °C for 48 h. Ethyl acetate (10 mL) was added, the reaction filtered, and the filtrate washed with water (3 × 20 mL) and brine (20 mL). The organic layer was dried over magnesium sulfate and evaporated under reduced pressure. Boiling ethyl acetate (2 mL) was added, and the mixture allowed to cool to room temperature, then in an ice bath. The precipitate was washed with cold ethyl acetate to yield a brown solid (74.3 mg, 49%). ^{1}H NMR (400 MHz, DMSO-d_6) δ 8.84 (s, 2H); 8.58 (d, J = 4.0 Hz, 2H); 8.06 (td, J = 4.0, 8.0 Hz, 2H); 7.47 (dd, J = 8.0, 8.0 Hz, 2H); 7.39 (d, J = 8.0 Hz, 2H); 6.64 (t, J = 8.0 Hz, 1H); 5.91 (s, 1H); ^{13}C (100 MHz, DMSO-d_6) δ 152.8; 150.1; 142.5; 133.9; 133.3; 129.2; 127.3; 122.3; 121.2; 93.7; 85.1. HRMS (ESI) m/z: calcd for $C_{20}H_{13}N_3$ (M + H$^+$) 296.1182; found 296.1118.

Complex [(6a)$_4$·Pd$_2$](NO$_3$)$_4$. ^{1}H NMR (400 MHz, DMSO-d_6) δ 9.66 (s, 2H); 9.36 (d, J = 8.0 Hz, 2H); 8.21 (d, J = 8.0 Hz, 2H); 7.79 (dd, J = 8.0, 8.0 Hz, 2H); 7.43 (d, J = 8.0 Hz, 2H); 6.67 (t, J = 8.0 Hz, 1H); 6.24 (s, 2H); ^{13}C (100 MHz, DMSO-d_6) δ 152.6, 150.5, 149.9, 142.0, 134.8, 127.2, 122.9, 116.9, 105.1, 92.4, 89.6. HRMS (ESI) (OTf$^-$ salt) m/z: calcd for $C_{83}H_{52}N_{12}O_9F_9S_3{}^{106}Pd^{108}Pd$ (M − OTf$^-$)$^+$ 1841.1067; found 1841.1054.

2,6-Bis(pyridylethynyl)-4-nitroaniline ***6b***. To an oven-dried 25 mL round-bottom flask with a magnetic stirring bar was added 2,6-diiodonitroaniline (390 mg, 1 mmol), 3-ethynylpyridine (250 mg, 2.4 mmol), bis(triphenylphosphine)-palladium(II) dichloride (20 mg), and triphenylphosphine (20 mg). The mixture was placed under nitrogen and diethylamine (5 mL) degassed was added by syringe. The reaction was heated to 70 °C for 18 h. Ethyl Acetate (50 mL) was added to the reaction mixture, and the mixture filtered. The filtration was subject to aqueous workup and extracted with ethyl acetate. The combined organic layer was dried over anhydrous sodium sulfate and evaporated under reduced pressure. The residue was purified by flash column chromatography on silica gel ($CHCl_3$, $CHCl_3$/methanol = 100:2, $CHCl_3$/methanol = 100:4) to yield a yellow solid (220 mg, 65%). ^{1}H NMR (400 MHz, DMSO-d_6) δ 8.92 (d, J = 1.9 Hz, 2H), 8.61 (dd, J = 1.6, 4.8 Hz, 2H), 8.24 (s, 2H), 8.14 (dt, J = 1.8, 7.9 Hz, 2H), 7.50 (dd, J = 5.0, 8.0 Hz, 2H), 7.28 (s, 2H). ^{13}C NMR (100 MHz, DMSO-d_6) δ 154.6, 152.1, 149.2, 138.9, 135.9, 129.1, 123.5, 119.2, 105.5, 92.6, 86.8. HRMS (ESI) m/z: calcd for $C_{20}H_{12}N_4O_2$ (M+H)$^+$ 341.1033; found 341.1009.

Complex [(6b)$_4$·Pd$_2$](NO$_3$)$_4$. ^{1}H NMR (400 MHz, DMSO-d$_6$) δ 9.68 (s, 2H); 9.40 (d, J = 4.0 Hz, 2H); 8.31 (d, J = 8.0 Hz, 2H); 8.29 (s, 2H); 7.85 (dd, J = 6.0, 8.0 Hz, 2H); 7.34 (s, 2H); ^{13}C NMR (125 MHz, DMSO-d$_6$) δ 154.5; 152.8; 150.5; 142.5; 136.5; 130.2; 127.3; 122.3; 105.1; 90.5; 89.9. HRMS (ESI) m/z: calcd for $C_{83}H_{48}N_{16}O_{17}F_9S_3{}^{106}Pd^{108}Pd$ (M − OTf$^-$)$^+$ 2021.0470; found 2021.0531.

4-Amino-3,5-bis(pyridin-3-ylethynyl)benzoic Acid ***6c***. To an oven-dried 25 mL round-bottomed flask equipped with stir bar and reflux condenser was added 4-amino-3,5-diiodobenzoic acid (195 mg, 0.501 mmol), 3-ethynylpyridine (130 mg, 1.261 mmol), bis(triphenylphosphine)palladium(II) dichloride (15 mg, 0.021 mmol), and triphenylphosphine (9 mg, 0.034 mmol). The mixture was placed under nitrogen, and dry, degassed THF (4 mL), and degassed triethylamine (4 mL) were added. The reaction was heated at 50 °C for 16 h. Tetrahydrofuran was added (20 mL), and the reaction filtered. The filtrate was evaporated under reduced pressure, and the residue purified by flash column chromatography on silica gel ($CHCl_3$/MeOH 100:4; $CHCl_3$/MeOH 100:10) to yield a yellow solid (65 mg, 38%). ^{1}H NMR (400 MHz, DMSO-d_6) δ 12.64 (br s, 1H); 8.89 (d, J = 1.2 Hz, 2H); 8.59 (dd, J = 1.6, 4.8 Hz, 2H); 8.11 (td, J = 2.0, 8.0 Hz, 2H); 7.91 (s, 2H); 7.48 (dd, J = 4.8, 8.0 Hz, 2H); 6.64 (s, 2H); ^{13}C NMR (100 MHz, DMSO- d_6) δ 165.9; 152.9; 151.9; 148.9; 138.7; 134.7; 123.4; 119.6; 118.1; 105.4; 91.7; 88.0; HRMS (ESI) m/z: calcd for $C_{21}H_{13}N_3O_2$ (M + H)$^+$ 340.1081; found 340.1073.

Complex [(6c)$_4$·Pd$_2$](NO$_3$)$_4$. ^{1}H NMR (400 MHz, DMSO-d_6) δ 9.68 (s, 2H); 9.37 (d, J = 5.2 Hz, 2H); 8.29 (d, J = 8.0 Hz, 2H); 7.96 (s, 2H); 7.81 (dd, J = 6.0, 7.6 Hz, 2H); 6.83 (s, 2H); HRMS (ESI) m/z: calcd for $C_{87}H_{52}N_{12}O_{17}F_9S_3{}^{106}Pd^{108}Pd$ (M − OTf$^-$)$^+$ 2017.0660; found 2017.0727. Note: this complex was too insoluble to obtain a ^{13}C NMR spectrum in any reasonable amount of time.

2,6-Bis(pyridin-3-ylethynyl)pyridine ***6d***. To an oven-dried 25 mL round-bottom flask with a magnetic stirring bar was added 2,6-dibromopyridine (471 mg, 2 mmol), 3-ethynylpyridine (500 mg, 4.8 mmol), bis(triphenylphosphine)-palladium(II) dichloride (40 mg), triphenylphosphine (30 mg), and copper iodide (15 mg). The mixture was placed under nitrogen, and diethylamine (12 mL) degassed were added by syringe. The reaction was heated to 60 °C under nitrogen for 18 h. Ethyl acetate (50 mL) was added to the reaction mixture, and the mixture filtered. The filtration was subject to aqueous workup and extracted with ethyl acetate. The combined organic layer was dried over anhydrous sodium sulfate and evaporated under reduced pressure. The residue was purified by flash column chromatography on silica gel ($CHCl_3$/methanol = 100:2) to yield a yellow solid (640 mg 50%). ^{1}H NMR (400 MHz, DMSO-d_6) δ 8.85 (s, 2H), 8.66 (d, J = 3.6 Hz, 2H), 8.08 (dt, J = 1.8, 7.9 Hz, 2H), 7.98 (t, J = 7.8 Hz, 2H), 7.74 (d, J = 7.8 Hz, 2H), 7.52 (dd, J = 4.9, 7.9 Hz, 2H). ^{13}C NMR (100 MHz, DMSO-d_6) δ 152.0; 149.8; 142.3; 139.1; 137.9; 127.4; 123.8; 118.3; 90.9; 85.8. HRMS (ESI) m/z: calcd for $C_{19}H_{11}N_3$ (M + H)$^+$ 282.1026; found 282.1002.

Complex [(6d)$_4$·Pd$_2$](NO$_3$)$_4$. ^{1}H NMR (400 MHz, DMSO-d$_6$) δ 9.88 (s, 2H), 9.41 (d, J = 5.3 Hz, 2H), 8.32 (d, J = 8.0 Hz, 2H), 7.97 (t, J = 7.8 Hz,

dx.doi.org/10.1021/ic201092s |*Inorg. Chem.* 2011, 50, 9430–9442

2H), 7.84 (dd, J = 5.9, 7.9 Hz, 2H), 7.75 (d, J = 7.8 Hz, 2H); ^{13}C NMR δ 153.5; 151.0; 143.3; 141.9; 138.0; 128.6; 127.3; 121.6; 93.3; 83.3. HRMS (ESI) m/z: calcd for $C_{79}H_{44}N_{12}O_9F_9S_3{}^{106}Pd^{108}Pd$ (M − OTf$^-$)$^+$ 1785.0441; found 1785.0473.

1,3-Bis((4-(pyridin-3-yl)phenyl)ethynyl)benzene ***8***. To an oven-dried, 50 mL round-bottom flask equipped with a magnetic stirrer was added 1,3-diethynylbenzene (300 mg, 0.24 mmol), 1-bromo-4-iodobenzene (1.365 g, 0.48 mmol), bis(triphenylphosphine)palladium(II) dichloride (168 mg), and CuI (23 mg). The mixture was placed under nitrogen and anhydrous diisopropylamine (20 mL) was added by syringe. The reaction was left to stir at room temperature for 30 h. The solvent was removed by rotary evaporation, and the remaining solid was dissolved in methylene chloride (10 mL). The mixture was then filtered through Celite, and the solvent from the filtrate was removed by rotary evaporation. Recrystallization from methylene chloride gave 1,3-bis((4-bromophenyl)-ethynyl)benzene (880 mg, 85%) as an off white powder. ^{1}H NMR (300 MHz, $CDCl_3$) δ 7.69 (br s, 1H), 7.51−7.45 (m, J = 8.67 Hz, 4 H), 7.40 (d, J = 8.23 Hz, 4 H), 7.34 (d, J = 7.68 Hz, 1 H). ^{13}C NMR (400 MHz, $CDCl_3$) δ 135.3; 134.6; 133.2; 131.7; 131.6; 123.5; 122.8; 122.0; 89.6. GCMS (EI) m/z: calcd for $C_{22}H_{12}Br_2$ (M+H$^+$) 433.9300; found 433.9283.

To an oven-dried, 25 mL round-bottom flask equipped with a magnetic stirrer was added 1,3-bis((4-bromophenyl)ethynyl)benzene (100 mg, 0.23 mmol) and 3-pyridine boronic acid **9** (59 mg, 0.48 mmol), bis(triphenylphosphine)palladium(II) dichloride (16 mg), and Cs_2CO_3 (450 mg, 1.4 mmol). The mixture was placed under nitrogen and degassed ethanol (4 mL) and anhydrous toluene (2 mL) were added by syringe. The reaction was stirred at 73 °C for 24 h. The solvent was removed by rotary evaporation, and the remaining solid was dissolved in methylene chloride (10 mL). The mixture was then filtered through Celite, and the solvent from the filtrate was removed by rotary evaporation. The crude product was purified by flash column chromatography on silica gel (CH_2Cl_2/methanol = 100:1) to yield compound **8** (30 mg, 10%) as a light brown solid. ^{1}H NMR (400 MHz, DMSO-d_6): δ 8.97 (s, 2H), 8.61 (d, J = 3.8 Hz, 2H), 8.16 (d, J = 8.6 Hz, 2H), 7.85 (d, J = 8.4 Hz, 4H), 7.81 (s, 1H), 7.73 (d, J = 8.5 Hz, 4H), 7.65 (d, J = 7.4 Hz, 2H), 7.55−7.51 (m, J = 6.6 Hz, 3H). ^{13}C NMR (100 MHz, $CDCl_3$): δ 148.7; 148.1; 137.8; 134.8; 134.5; 132.5; 132.1; 131.6; 129.8; 128.7; 127.2; 123.6; 123.1; 89.9; 89.7. HRMS (ESI) m/z: calcd for $C_{32}H_{20}N_2$ (M + H$^+$) 432.1621; found at 432.1614.

Complex [8$_4$·Pd$_2$](NO$_3$)$_4$. ^{1}H NMR (100 MHz, DMSO-d_6): δ 9.98 (s, 8H), 9.42 (d, J = 5.9 Hz, 8H), 8.48 (d, J = 8.3 Hz, 8H), 7.94 (d, J = 8.4 Hz, 16H), 7.88 (m, J = 6.9 Hz, 8H), 7.81 (d, J = 8.2 Hz, 18H), 7.74 (s, 4H), 7.62 (d, J = 1.1 Hz, 8H), 7.51 (t, J = 7.2 Hz, 4H). ^{13}C NMR (125 MHz, DMSO-d_6): δ 149.9; 148.6; 138.4; 137.6; 134.4; 133.8; 131.9; 129.6; 127.4; 127.3; 123.2; 122.6; 90.1; 89.5. HRMS (ESI) m/z: calcd for $C_{130}H_{81}N_8O_6F_6S_2{}^{106}Pd^{108}Pd$ (M − 2OTf$^-$)$^{2+}$ 1120.6844; found at 1120.6888. Note: in this case the monocation was not observed, and the MS data for the dication is shown.

3-((4-Bromophenyl)ethynyl)pyridine ***10***. To an oven-dried, 50 mL round-bottom flask equipped with a magnetic stirrer was added 3-ethynyl pyridine (180 mg, 1.7 mmol), 1-bromo-4-iodobenzene (406 mg, 1.4 mmol), bis(triphenylphosphine)palladium(II) dichloride (52 mg), and CuI (8 mg). The mixture was placed under nitrogen and anhydrous diisopropylamine (3 mL) were added by syringe. The reaction was left to stir at room temperature for 24 h. The solvent was removed by rotary evaporation, and the remaining solid was dissolved in methylene chloride (10 mL). The mixture was then filtered through Celite, and the solvent from the filtrate was removed by rotary evaporation to yield 3-((4-bromophenyl)ethynyl)pyridine **10** (277 mg, 75%). ^{1}H NMR (400 MHz, $CDCl_3$): δ 8.77 (s, J = 1.04, 1H), 8.57 (d, J = 4.9 Hz, 1H), 7.8 (d, J = 7.8 Hz, 1H), 7.53 (d, J = 8.7 Hz, 1H), 7.42 (d, J = 8.7 Hz, 1H), 7.32−7.27 (m, 1H). ^{13}C NMR (100 MHz, $CDCl_3$): δ 152.2; 148.8; 138.5; 133.2; 131.8; 123.2; 121.5; 120.3; 91.7; 87.0. HRMS (ESI) m/z: calcd for $C_{13}H_8BrN$ (M+H$^+$) 256.9835; found at 256.9836.

1,3-Bis((4-(pyridin-3-ylethynyl)phenyl)ethynyl)benzene ***11***. To an oven-dried, 25 mL round-bottom flask equipped with a magnetic stirrer was added 1.3 diethynyl benzene (40 mg, 0.32 mmol), 3-((4-bromophenyl)-ethynyl)pyridine **10** (166 mg, 0.64 mmol), bis(triphenylphosphine)-palladium(II) dichloride (2.2 mg), and CuI (3 mg). The mixture was placed under nitrogen, and anhydrous diisopropylamine (3 mL) was added by syringe. The reaction was stirred at room temperature for 24 h. The solvent was removed by rotary evaporation, and the remaining solid was dissolved in methylene chloride (10 mL). The mixture was then filtered through Celite, and the solvent from the filtrate was removed by rotary evaporation to yield 1,3-bis((4-(pyridin-3-ylethynyl)phenyl)ethynyl)-benzene **11** (42 mg, 27%). ^{1}H NMR (400 MHz, $CDCl_3$): δ 8.78 (s, 2H), 8.58 (d, J = 4.8 Hz, 2H), 7.83 (d, J = 7.9 Hz, 2H), 7.72 (s, 1H), 7.53 (s, 8H), 7.51 (d, J = 7.8 Hz, 2H), 7.382 (t, J = 7.1 Hz, 1H), 7.32 (m, J = 7.8 Hz, 2H). LIFDI-MS m/z: calcd for $C_{36}H_{20}N_2$ (M+H$^+$) found at 480.

Complex [11$_4$·Pd$_2$](NO$_3$)$_4$. ^{1}H NMR (400 MHz, DMSO-d_6): δ 9.60 (s, 8H), 9.29 (d, J = 8.52, 8H), 7.82−7.43 (m, 60H). This complex was poorly stable, and HRMS/^{13}C data could not be obtained.

X-RAY STRUCTURE DETERMINATION

Crystal Data. A light yellow fragment of a prism (0.43 × 0.27 × 0.18 mm^3) was used for the single crystal X-ray diffraction study of $[C_{80}H_{52}N_{12}Pd_2]^{4+}[CF_3SO_3]_4^-$. The crystal was coated with paratone oil and mounted onto a cryo-loop glass fiber. X-ray intensity data were collected at 100(2) K on a Bruker APEX2 platform-CCD X-ray diffractometer system (fine focus Mo-radiation, λ = 0.71073 Å, 50KV/30 mA power). The CCD detector was placed at a distance of 4.9890 cm from the crystal. $[C_{80}H_{52}N_{12}Pd_2]^{4+}[CF_3SO_3]^-{}_4$[partial solvents] M = 2111.77 [including partially occupied solvents], CCDC submission no. 828749, triclinic space group $P\bar{1}$ (no. 2), **a** = 12.6089(15) Å, **b** = 19.950(2) Å, **c** = 21.233(3) Å, α = 63.3356(16)°, β = 73.1549(17)°, γ = 75.7105(17)°, V = 4525.4(9) Å^3, Z = 2, calculated density D_c = 1.550 g/cm^3, light yellow prism fragment (0.43 × 0.27 × 0.18 mm^3) coated with paratone oil, T = 100(2) K, 36788 reflections measured (0.73 Å resolution), 25380 unique (R_{int} = 0.0461, completeness = 99.6%), final $R1$ = 0.0685, $wR2$ = 0.1647 with intensity $I > 2\sigma(I)$ (see Supporting Information for full experimental details).

Procedure for Kinetics Measurements. *Addition of Ligand* ***6d*** *to Complex* ***[(3a)$_4$·Pd$_2$](NO$_3$)$_4$***. Ligand **3a** was dissolved in DMSO-d_6 to make a 14 mM solution, and a 152 mM solution of $Pd(NO_3)_2$ was titrated in until complex formation was almost complete. A portion of this solution was added to an equal volume 28 mM solution of ligand **6d**. After mixing, spectra were periodically acquired (3 s delay, 32 scans). Concentrations of ligands and complexes were measured by integrating the peaks at 8.78, 8.85, and 9.94−9.61.

Addition of Ligand ***6a*** *to Complex* ***[(3a)$_4$·Pd$_2$](NO$_3$)$_4$***. Ligand **3a** was dissolved in 500 μL of DMSO-d_6 to make a 14 mM solution, and a 152 mM solution of $Pd(NO_3)_2$ was titrated in until complex formation was complete. A portion of this solution was added to an equal volume 28 mM solution of ligand **6a**. After mixing, spectra were periodically acquired (3 s delay, 32 scans). Concentrations of ligands and complex were measured by integrating the peaks at 8.00, 8.06, and 9.59−9.80 ppm.

Procedure for Diffusion Experiments. Diffusion experiments were performed using a Bruker Avance 600 MHz NMR spectrometer equipped with a broadband inverse probe with x-, y-, and z-gradients. Chemical shifts were referenced to the

dimethyl sulfoxide-d^5 resonance (2.504) ppm. Diffusion data sets were acquired using the stimulated echo experiment with bipolar gradients (stebpgp1s) included with the Topspin release version 1.3. Gradient amplitudes were incremented as a square dependence from 5% to 95% into 22 gradient increments. A spoil gradient pulse of length 1 ms and amplitude of −17.13% was used to effectively remove transverse magnetization following the encode period of the pulse program. Spectra were acquired with 128 transients coadded and 28,672 data points per transient for each of the 22 increments. Diffusion (Δ) and gradient pulse times (δ) were optimized using a one-dimensional version of the stimulated echo pulse sequence, stebpgp1s1d to give values of 2.0 and 200 ms, respectively.

Following acquisition, the FIDs were apodized by multiplication with an exponential function equivalent to 1 Hz line broadening prior to processing in Topspin to obtain pseudo-2D DOSY plots. Diffusion coefficients were calculated using the DOSY Toolbox software.[34] To simplify analysis of the diffusion coefficients, processing was carried out on individual spectral regions corresponding to the resonances at 9.679, 9.391, 8.914, and 8.609 ppm. Analysis of the diffusion coefficients was carried out on individual spectral regions corresponding to the resonances at 9.679, 9.391, 8.914, and 8.609 ppm. The data was fit using a standard monoexponential decay with a diffusion resolution of 256 points. Fitting statistics for the pure exponential fitting to the Stejskal-Tanner equation for the diffusion coefficients and fitting errors were determined and displayed following DOSY processing.

Procedure for UV−vis and Fluorescence Experiments. Spectrophotometric grade dimethylsulfoxide was purchased from Aldrich and used as received. Each ligand stock solution was prepared at 7×10^{-3} M (3.5×10^{-6} mol of ligand in 5 mL of DMSO) and kept in the dark. For measurements, solutions of the ligands were freshly prepared from stock solutions by five to seven dilution steps such that, depending on the ligand, the concentration of each ligand solution was 2.2×10^{-5} M, unless otherwise stated. Each ligand was excited at λ_{exc} obtained from UV−vis measurement data, and emission spectra were recorded. A 3.5×10^{-3} M stock solution was prepared by dissolving 8 mg of $Pd(NO_3)_2$ (3.5×10^{-5} mol in 10 mL of DMSO) and was kept in the dark. One equivalent of metal solution was added to each ligand solution using a 25 μL syringe.

■ ASSOCIATED CONTENT

Supporting Information. NMR Spectra, fitted diffusion analysis, tabulated rate data, and X-ray Crystallographic analysis. This material is available free of charge via the Internet at http://pubs.acs.org.

■ AUTHOR INFORMATION

Corresponding Author
*E-mail: richard.hooley@ucr.edu.

■ ACKNOWLEDGMENT

We are grateful to the American Chemical Society Petroleum Research Fund, UC Riverside, and the NSF-funded ACIF (NSF CHE-9974924) for financial support. C.K.L. gratefully acknowledges financial support from the National Science Foundation Grant CHE 0848976. J.F.K.L. acknowledges support by a 2008-2010 U.S. Pharmacopeia graduate fellowship. A.S.G. acknowledges support by a 2010 GRMP graduate fellowship. The authors thank Prof. Christopher Bardeen for stimulating discussions.

■ REFERENCES

(1) Baxter, P.; Lehn, J.-M.; DeCian, A. *Angew. Chem., Int. Ed. Engl.* **1993**, *32*, 69–72.
(2) Caulder, D. L.; Raymond, K. N. *Acc. Chem. Res.* **1999**, *32*, 975–982.
(3) Saalfrank, R. W.; Maid, H.; Scheurer, A. *Angew. Chem., Int. Ed.* **2008**, *47*, 8794–8824.
(4) Fujita, M.; Umemoto, K.; Yoshizawa, M.; Fujita, N.; Kusukawa, T.; Biradha, K. *Chem. Commun.* **2001**, 509–518.
(5) Northrop, B. H.; Zheng, Y.-R.; Chi, K.-W.; Stang, P. J. *Acc. Chem. Res.* **2009**, *42*, 1554–1563.
(6) (a) Saalfrank, R. W.; Scheurer, A.; Puchta, R.; Hampel, F.; Maid, H.; Heinemann, F. W. *Angew. Chem., Int. Ed.* **2007**, *46*, 265–268. (b) Saalfrank, R. W.; Schmidt, C.; Maid, H.; Hampel, F.; Bauer, W.; Scheurer, A. *Angew. Chem., Int. Ed.* **2006**, *45*, 315–318. (c) Saalfrank, R. W.; Demleitner, B.; Glaser, H.; Maid, H.; Bathelt, D.; Hampel, F.; Bauer, W.; Teichert, M. *Chem.—Eur. J.* **2002**, *8*, 2679–2683. (d) Saalfrank, R. W.; Hörner, B.; Stalke, D.; Salbeck, J. *Angew. Chem., Int. Ed. Engl.* **1993**, *32*, 1179–1182. (e) Liu, T.; Liu, Y.; Xuan, W.; Cui, Y. *Angew. Chem., Int. Ed.* **2010**, *49*, 4121–4124. (f) Schultheiss, N.; Ellsworth, J. M.; Bosch, E.; Barnes, C. L. *Eur. J. Inorg. Chem.* **2005**, 45–46.
(7) (a) Fiedler, D.; Leung, D. H.; Bergman, R. G.; Raymond, K. N. *Acc. Chem. Res.* **2005**, *38*, 351–360. (b) Beissel, T.; Powers, R. E.; Raymond, K. N. *Angew. Chem., Int. Ed. Engl.* **1996**, *35*, 1084–1086. (c) Biros, S. M.; Bergman, R. G.; Raymond, K. N. *J. Am. Chem. Soc.* **2007**, *129*, 12094–12095. (d) Dong, V. M.; Fiedler, D.; Carl, B.; Bergman, R. G.; Raymond, K. N. *J. Am. Chem. Soc.* **2006**, *128*, 14464–14465. (e) Mugridge, J. S.; Szigethy, G.; Bergman, R. G.; Raymond, K. N. *J. Am. Chem. Soc.* **2010**, *132*, 16256–16264.
(8) (a) Mal, P.; Schultz, D.; Beyeh, K.; Rissanen, K.; Nitschke, J. R. *Angew. Chem., Int. Ed.* **2008**, *47*, 8297–8301. (b) Mal, P.; Breiner, B.; Rissanen, K.; Nitschke, J. R. *Science* **2009**, *324*, 1697–1699. (c) Riddell, I. A.; Smulders, M. M. J.; Clegg, J. K.; Nitschke, J. R. *Chem. Commun.* **2011**, *47*, 457–459. (d) Meng, W.; Breiner, B.; Rissanen, K.; Thoburn, J. D.; Clegg, J. K.; Nitschke, J. R. *Angew. Chem., Int. Ed.* **2011**, *50*, 3479–3483.
(9) (a) Fujita, M.; Oguro, D.; Miyazawa, M.; Oka, H.; Yamaguchi, K.; Ogura, K. *Nature* **1995**, *378*, 469–471. (b) Aoyagi, M.; Biradha, K.; Fujita, M. *J. Am. Chem. Soc.* **1999**, *121*, 7457–7458. (c) Yamanoi, Y.; Sakamoto, Y.; Kusukawa, T.; Fujita, M.; Sakamoto, S.; Yamaguchi, K. *J. Am. Chem. Soc.* **2001**, *123*, 980–981. (d) Ono, K.; Yoshizawa, M.; Kato, T.; Watanabe, K.; Fujita, M. *Angew. Chem., Int. Ed.* **2007**, *46*, 1803–1806. (e) Nishioka, Y.; Yamaguchi, T.; Kawano, M.; Fujita, M. *J. Am. Chem. Soc.* **2008**, *130*, 8160–8161. (f) Sato, S.; Ishido, Y.; Fujita, M. *J. Am. Chem. Soc.* **2009**, *131*, 6064–6065. (g) Yamauchi, Y.; Yoshizawa, M.; Akira, M.; Fujita, M. *J. Am. Chem. Soc.* **2010**, *132*, 960–966. (h) Sun, Q.-F.; Iwasa, J.; Ogawa, D.; Ishido, Y.; Sato, S.; Ozeki, T.; Sei, Y.; Yamaguchi, K.; Fujita, M. *Science* **2010**, *328*, 1144–1147.
(10) (a) Clever, G. H.; Shionoya, M. *Chem.—Eur. J.* **2010**, *16*, 11792–11796. (b) Clever, G. H.; Tashiro, S.; Shionoya, M. *Angew. Chem., Int. Ed.* **2009**, *48*, 7010–7012. Clever, G. H.; Shionoya, M. *J. Am. Chem. Soc.* **2010**, *132*, 9973–9975.
(11) (a) Leininger, S.; Olenyuk, B.; Stang, P. J. *Chem. Rev.* **2000**, *100*, 853–908. (b) Wang, M.; Zheng, Y.-R.; Ghosh, K.; Stang, P. J. *J. Am. Chem. Soc.* **2010**, *132*, 6282–6283. (c) Lee, J.; Ghosh, K.; Stang, P. J. *J. Am. Chem. Soc.* **2009**, *131*, 12028–12029. (d) Zhao, L.; Northrop, B. H.; Stang, P. J. *J. Am. Chem. Soc.* **2008**, *130*, 11886–11888.
(12) (a) Davis, A. V.; Fiedler, D.; Seeber, G.; Zahl, A.; van Eldik, R.; Raymond, K. N. *J. Am. Chem. Soc.* **2006**, *128*, 1324–1333. (b) Sgarlata, C.; Mugridge, J. S.; Pluth, M. D.; Tiedemann, B. E. F.; Zito, V.; Arena, G.; Raymond, K. N. *J. Am. Chem. Soc.* **2010**, *132*, 1005–1009.
(13) (a) Yoshizawa, M.; Tamura, M.; Fujita, M. *Science* **2006**, *312*, 251–254. (b) Pluth, M. D.; Bergman, R. G.; Raymond, K. N. *Science* **2007**, *316*, 85–88.

(14) (a) Fiedler, D.; Bergman, R. G.; Raymond, K. N. *Angew. Chem., Int. Ed.* **2004**, *43*, 6748–6755. (b) Hastings, C. J.; Pluth, M. D.; Bergman, R. G.; Raymond, K. N. *J. Am. Chem. Soc.* **2010**, *132*, 6938–6940. (c) Fiedler, D.; van Halbeek, H.; Bergman, R. G.; Raymond, K. N. *J. Am. Chem. Soc.* **2006**, *128*, 10240–10252.

(15) (a) Sato, S.; Iida, J.; Suzuki, K.; Kawano, M.; Ozeki, T.; Fujita, M. *Science* **2006**, *313*, 1273–1276. (b) Suzuki, K.; Iida, J.; Sato, S.; Kawano, M.; Fujita, M. *Angew. Chem., Int. Ed.* **2008**, *47*, 5780–5782. (c) Suzuki, K.; Kawano, M.; Sato, S.; Fujita, M. *J. Am. Chem. Soc.* **2007**, *129*, 10652–10653. (d) Sato, S.; Ishido, Y.; Fujita, M. *J. Am. Chem. Soc.* **2009**, *131*, 6064–6065. (e) Zhao, L.; Ghosh, K.; Zheng, Y.-R.; Stang, P. J. *J. Org. Chem.* **2009**, *74*, 8516–8521. (f) Caskey, D. C.; Yamamoto, T.; Addicott, C.; Shoemaker, R. K.; Vacek, J.; Hawkridge, A. M.; Muddiman, D. C.; Kottas, G. S.; Michl, J.; Stang, P. J. *J. Am. Chem. Soc.* **2008**, *130*, 7620–7628.

(16) (a) Hooley, R. J.; Rebek, J., Jr. *Chem. Biol.* **2009**, *16*, 255–264. (b) Renslo, A. R.; Rebek, J., Jr. *Angew. Chem., Int. Ed.* **2000**, *39*, 3281–3283. (c) Iwasawa, T.; Hooley, R. J.; Rebek, J., Jr. *Science* **2007**, *317*, 493–496. (d) Hooley, R. J.; Iwasawa, T.; Rebek, J., Jr. *J. Am. Chem. Soc.* **2007**, *129*, 15330–15339. (e) Purse, B. W.; Ballester, P.; Rebek, J., Jr. *J. Am. Chem. Soc.* **2003**, *125*, 14682–14683. (f) Mastalerz, M. *Chem. Commun.* **2008**, 4759–4758.

(17) (a) Yang, H.-B.; Ghosh, K.; Zhao, Y.; Northrop, B. H.; Lyndon, M. M.; Muddiman, D. C.; White, H. S.; Stang, P. J. *J. Am. Chem. Soc.* **2008**, *130*, 839–841. (b) Ghosh, K.; Hu, J.; White, H. S.; Stang, P. J. *J. Am. Chem. Soc.* **2009**, *131*, 6695–6697. (c) Vacek, J.; Caskey, D. C.; Horinek, D.; Shoemaker, R. K.; Stang, P. J.; Michl, J. *J. Am. Chem. Soc.* **2008**, *130*, 7629–7638. (d) Yang, H.-B.; Hawkridge, A. M.; Huang, S. D.; Das, N.; Bunge, S. D.; Muddiman, D. C.; Stang, P. J. *J. Am. Chem. Soc.* **2007**, *129*, 2120–2129.

(18) Wang, Z.; Cohen, S. M. *Chem. Soc. Rev.* **2009**, *38*, 1315–1329.

(19) (a) A portion of this work has been previously communicated: Liao, P.; Langloss, B. W.; Johnson, A. M.; Knudsen, E. R.; Tham, F. S.; Julian, R. R.; Hooley, R. J. *Chem. Commun.* **2010**, *46*, 4932–4934.

(20) Similar ligands are capable of complexation with silver ions to form macrocycles: Kilpin, K. J.; Gower, M. L.; Telfer, S. G.; Jameson, G. B.; Crowley, J. D. *Inorg. Chem.* **2011**, *50*, 1123–1134.

(21) Chinchilla, R.; Nájera, C. *Chem. Rev.* **2007**, *107*, 874–922.

(22) Surry, D. S.; Buchwald, S. L. *Angew. Chem., Int. Ed.* **2008**, *47*, 6338–6361.

(23) Iritani, K.; Matsubara, S.; Uchimoto, K. *Tetrahedron Lett.* **1988**, *29*, 1799–1802.

(24) Yue, N. L. S.; Eisler, D. J.; Jennings, M. C.; Puddephatt, R. J. *Inorg. Chem.* **2004**, *43*, 7671–7681.

(25) Kim, H.-J.; Lee, E.; Kim, M. G.; Kim, M.-C.; Lee, M.; Sim, E. *Chem.—Eur. J.* **2008**, *14*, 3883.

(26) (a) Tanner, J. E. *J. Chem. Phys.* **1970**, *52*, 2523–2526. (b) Wu, D. H.; Chen, A. D.; Johnson, C. S. *J. Magn. Reson., Ser. A* **1995**, *115*, 260–264. (c) Pelta, M. D.; Barjat, H.; Morris, G. A.; Davis, A. L.; Hammond, S. J. *Magn. Reson. Chem.* **1998**, *36*, 706–714. (d) Otto, W. H.; Keefe, M. H.; Splan, K. E.; Hupp, J. T.; Larive, C. K. *Inorg. Chem.* **2002**, *41*, 6172–6174.

(27) The projection in the diffusion dimension (F1) corresponds to peaks in the chemical shift region (F2) between 10 ppm and 8.5 ppm. This region was selected to remove the contribution from the large singlet at 8.28 ppm belonging to the complex and more easily resolve the peak from **6b** in the diffusion projection plotted along the *y*-axis.

(28) The NMR spectra of the Pd_2L_4OTf salts were similar to the nitrate spectra shown; $Pd(NO_3)_2$ was used for the NMR analysis because of increased ease of handling.

(29) Johnson, A. M.; Hooley, R. J. *Inorg. Chem.* **2011**, *50*, 4671–4673.

(30) Zheng, Y.-R.; Stang, P. *J. Am. Chem. Soc.* **2009**, *131*, 3487–3489.

(31) (a) Lentijo, S.; Miguel, J. A.; Espinet, P. *Organometallics* **2011**, *30*, 1059–1066. (b) Eryazici, I.; Moorefield, C. N.; Newkome, G. R. *Chem. Rev.* **2008**, *108*, 1834–1895. (c) Devi, U.; Brown, J. R. D.; Almond, A.; Webb, S. J. *Langmuir* **2011**, *27*, 1448–1456.

(32) Murata, S.; Ido, Y. *Bull. Chem. Soc. Jpn.* **1994**, *67*, 1746–1748.

(33) Dewar, M. J. S.; Zoebisch, E. G.; Healy, E. F.; Stewart, J. J. P. *J. Am. Chem. Soc.* **1985**, *107*, 3902–3909.Calculations were performed on *SPARTAN 06*; Wavefunction Inc: Irvine, CA, 2006.

(34) Nilsson, M. *J. Magn. Reson.* **2009**, *200*, 296–302.